

Trace and rare earth element geochemistry of the Oligocene Nikopol stratiform manganese oxide-hydroxide ores, Ukraine

Ahmet SASMAZ¹, Vasyi M Zagnitko², and Bilge SASMAZ³

¹Firat University

²Taras Shevchenko National University of Kyiv

³Firat University

November 23, 2022

Abstract

The Nikopol manganese deposit is one of the world's largest deposits among the sedimentary manganese deposits. The Nikopol Oligocene basin is located between the Azov crystalline massif and the Ukrainian shield. Nikopol Ore horizon is traced in a thickness varying from several cm to 4.5 m and a single stratum from the west to the eastwards to about 250 km and separated to three different units; carbonate, mixed carbonate-oxide, and oxide ore. The oxide ores can contain the concretion or earthy masses bigger than 25 cm, sometimes with remnants of carbonate or carbonate-oxide textures. The manganese oxide-hydroxide ores were analyzed for major oxides, trace and rare earth elements (REE) using ICP-MS. The PAAS-normalized REE patterns of the Nikopol manganese oxide ores have similar trends and show MREE and HREEs enrichments. The Ce/Ce* values of manganese oxide-hydroxide ores collected from the study area vary from 0.88 to 1.43, indicating that ore-forming rocks were primarily marine chemical or biogenic deposit. The Eu/ Eu* anomalies of the manganese oxide-hydroxide ores are close to 1. The Y concentrations vary from 9,1 to 47,1 ppm and show negative Y anomalies. Both geochemical and Pb isotope data indicate that the Nikopol manganese oxide-hydroxide ores formed rapidly within oxic/suboxic seawater as reflected by Ce anomalies close to 1 in low-oxygen fugacity in source of the hydrothermal fluids, volcanogenic input or hydrothermal contributions to seawater. Also, our results point out that the metal was transported from both a hydrothermal source in deeper water and terrestrial sources.

Trace and rare earth element geochemistry of the Oligocene Nikopol stratiform manganese oxide-hydroxide ores, Ukraine

Ahmet Sasmaz^{a*}, Vasyl M. Zagnitko^b, Bilge Sasmaz^a

^{a*} Department of Geological Engineering, Firat University 23119, Elazig, Turkey

^b Taras Shevchenko National University of Kyiv, Institute of Geology, 90 Vasylykivska, Kiev, Ukraine

Abstract

The Nikopol manganese deposit is one of the world's largest deposits among the sedimentary manganese deposits. The Nikopol Oligocene basin is located between the Azov crystalline massif and the Ukrainian shield. Nikopol Ore horizon is traced in a thickness varying from several cm to 4.5 m and a single stratum from the west to the eastwards to about 250 km and separated to three different units; carbonate, mixed carbonate-oxide, and oxide ore. The oxide ores can contain the concretion or earthy masses bigger than 25 cm, sometimes with remnants of carbonate or carbonate-oxide textures. The manganese oxide-hydroxide ores were analyzed for major oxides, trace and rare earth elements (REE) using ICP-MS. The PAAS-normalized REE patterns of the Nikopol manganese oxide ores have similar trends and show MREE and HREEs enrichments. The Ce/Ce* values of manganese oxide-hydroxide ores collected from the study area vary from 0.88 to 1.43, indicating that ore-forming rocks were primarily marine chemical or biogenic deposit. The Eu/ Eu* anomalies of the manganese oxide-hydroxide ores are close to 1. The Y concentrations vary from 9,1 to 47,1 ppm and show negative Y anomalies. Both geochemical and Pb isotope data indicate that the Nikopol manganese oxide-hydroxide ores formed rapidly within oxic/suboxic seawater as reflected by Ce anomalies close to 1 in low-oxygen fugacity in source of the hydrothermal fluids, volcanogenic input or hydrothermal contributions to seawater. Also, our results point out that the metal was transported from both a hydrothermal source in deeper water and terrestrial sources.

Key words: Manganese oxide ore, trace element, rare earth element, Nikopol, Ukraine

Plain Language Summary

Manganese occurs in many minerals such as manganite, sugilite, purpurite, rhodonite, rhodochrosite, and pyrolusite. The most important use of manganese is in the manufacturing of steel. Currently, steel production accounts for 85 to 90% of total manganese consumption. Manganese is often used by the steel industry in deoxidizing, desulfurizing additives and dry cell batteries. It can improve the rolling and forging qualities, as well as the strength, toughness, stiffness, hardness, wear resistance, and hardenability of steels. As a result, manganese is one of the indispensable elements of technology and will continue to be widely used in the future. For this reason, manganese beds will become much more important in the coming years. Sedimentary manganese deposits produce the bulk

37 of the world's output of manganese. These deposits in Ukraine, Georgia and Russia are the world
38 leader in manganese ore production with about 45% of world production. Approximately 75% of this
39 came from the Nikopol in the Ukraine and much of remainder from the Chiatura Basin in Georgia. For
40 these reasons, it becomes clear how important the investigation of Nikopol sedimentary manganese
41 deposits is.
42

43 1. INTRODUCTION

44 The Nikopol manganese deposits are located in the Eastern Paratethys basin the Nikopol, at the
45 southeast of Ukraine and one of the largest manganese deposits of metallurgical manganese in the world among
46 the sedimentary manganese deposits. The deposits were discovered in 1883 and production began in 1886 and
47 the total area of explored deposits is about 500 km². The ore body is almost horizontal or with a slight (up to 5⁰)
48 dips south or southwest. The ore is at 10- to 100-m depth. The thickness of ore varies from 0.5 to 5 m, and on
49 the average is 1.5 to 2.5 m thick. The manganese ore layer is characterized by inter stratification of the ore with
50 sand-silt clay sediments. The estimated total reserves of manganese ore around the Nikopol are calculated to be
51 626 million tons with grades between 10 and 45% in oxide ore, up to 30% in carbonate ore (Strishkov and
52 Levine, 1987). These deposits are known such giant deposits as Nikopol, Tokmak, Chiatura, Varna,
53 Mangyshlak, Binkilic, Laba, small deposits of Hungary and Slovakia formed in regional palaeogeographic
54 setting of the Early Oligocene of the Eastern Paratethys (Fig 1) (Kuleshov, 2017).

55 Based on the chemical composition and geological settings of Fe-Mn deposits, they can be divided to
56 three main groups: diagenetic, hydrogenetic, and hydrothermal (Hein et al., 1997; Bau et al., 2014; Josso et al.,
57 2017). Mn-Fe oxides form along the rock surfaces in the global ocean or sea at water depths between 400 and
58 7000 m. They extremely slowly develop by the collecting of colloids onto rock surfaces and the precipitation of
59 metals from bottom sea water, or by a contribution of hydrothermal and hydrogenetic precipitation in
60 hydrothermal vent areas (Hein et al., 2000). Manganese minerals in sedimentary environments may contain the
61 rare earth element (REE) concentrations in different rates (Chakhmouradian and Wall, 2012) due to ion
62 substitutions (Dill et al., 2011) or through sorption on Mn oxides. Manganese deposits and their REE
63 geochemistry have been used to better understand the geochemical and sedimentological conditions during the
64 formation of manganese minerals and their host rocks (McLennan, 1989; Dubinin, 2006; Hein et al., 2013; Hein
65 and Koschinsky, 2014; Sasmaz et al., 2014; Hein et al., 2017; Konstantinova et al., 2017; Chen et al., 2018;
66 Vereshchagin et al., 2019). The REE concentration in manganese deposits has been extensively used to
67 determine the genesis of hydrothermal systems and the physicochemical parameters of depositional
68 environments (Roy et al., 2018; Tobia, 2018; Sinanoglu and Sasmaz, 2019) in various depositional settings
69 (Akgul, 2015; Sasmaz et al., 2018). The Oligocene manganese oxide deposits in Nikopol and Chiatura contains
70 the main reserves of the world's onshore reserves of manganese (Maynard, 1983). The petrography and
71 mineralogy of both deposits were extensively studied during the Soviet Union period by various researchers
72 (Varentsov and Rakhmanov, 1980; Bolton and Frakes, 1985; Hein and Bolton, 1994) but no geochemical data

73 about trace and rare earth element contents were provided for these deposits. Here, we investigated the physico-
74 chemical conditions, the conditions of formation of the Nikopol manganese oxide/hydroxide deposit, and the
75 abundances of major oxide, trace elements, and REE concentration at various levels within the manganese
76 deposit.

77

78 **2. GEOLOGICAL SETTING OF THE NIKOPOL MANGANESE DEPOSIT**

79 The Eastern Paratethys contains many manganese deposits such as Ukraine (Tokmak and Nikopol);
80 Georgia (Chiatura and Kvirila); Bulgaria (Varna); Kazakhstan (Mangyshlak); Turkey (Binkilic); North
81 Caucasus (Laba deposits), Hungary and Slovakia) (Fig. 1). Manganese deposits formed in climatic, facies and
82 paleogeographic environments like Nikopol are also found in other places such as the Northern Ural region,
83 Europe, China, and North America. Nikopol and Tokmak deposits have more than 1 billion tons of Mn reserves
84 (Kuleshov, 2017).

85 The Nikopol Oligocene basin is located in the northeast part of the Black Sea tectonic depression zone
86 between the Azov crystalline massif in the east and the Ukrainian crystalline shield in the north (Fig. 1).
87 Manganese ores in Nikopol basin are formed in the Oligocene coastal-marine sediments related with the
88 stratigraphic sequence of the Black Sea depression (Kuleshov, 2017). Oligocene marine basin is a single basin
89 as structural, stratigraphic, and genetic (Fig. 2). All separate ore-bearing parts in this basin are parts of a same
90 system in Oligocene basin. The Nikopol Oligocene basin consists of two structural stages. These are the
91 crystalline basement rocks with Precambrian and sedimentary cover rocks from the Cretaceous to Quaternary.
92 This sedimentary cover rocks are with slope gradually to south-westerly direction (Fig. 3). The unity and
93 thickness of the sequence increase along this same direction. From the north to the south, the shallow water
94 coastal facies of the continental facies are observed first, and further to the south, deep-sea water facies are
95 observed. Oligocene deposits in the upper Cretaceous-Eocene basin lie on the crystalline basement rocks or their
96 weathering crust (Fig. 3). These deposits consist of three distinct members like a subore sands, Mn ores and
97 supra oreclays from the bottom to upwards. The manganese ore of the Nikopol basin has a single ore level
98 extending from west to east over a distance of about 250 km, with a thickness ranging from a few centimeters to
99 4.5 m (Fig. 3;4). This layer occurs from a sandstone-clay stratum representing a friable manganese ores and
100 concretionary manganese carbonate nodules. The concretion sizes vary to several dozens of centimeters from
101 several millimeters up. Manganese carbonate concretions in a length up to several hundred meters have
102 lensoidal structure with frequently intergrown in the host rocks. Manganese ores consist of either the oxides or
103 carbonates or their mixing of oxides and carbonates. A mineral zonality at the Nikopol' deposits is observed that
104 either along the sequence of the ore body from bottom toward top or in the replacement of oxide ores by
105 carbonate ores in the direction into the depth of the basin from the shore of the Oligocene basin. A typical
106 geological cross section for I and II oxide ore areas of the Nikopol manganese deposit is seen in Fig 2 (Strakhov
107 et al., 1968; taken from Kuleshov, 2017). The common and dominant ore in this basin is carbonate type ore.
108 Carbonate ores form a significant part of the ores in the Nikopol region; especially the main reserves are
109 observed in the Bolshoi Tokmak deposits in the east of this region (Fig. 2). Nikopol manganese ore horizon was

110 separated to three different units by Vorontsov and Rakhmanov (1977); carbonate ore, mixed carbonate-oxide
111 ore, and oxide ore. The carbonate ore shows in the most distal location from the continent and in two textural
112 changes: nodular-concretionary ores in 1 to 25 cm in diameter in a lumpy - coarse ores that have a clay-silt
113 matrix with highly porous texture. Both manganoan calcite and rhodochrosite are always reported to be very
114 fine-grained and poorly crystalline. The carbonate ore facies show the nodular changes such as fish bones,
115 sponge spicules and diatoms but the lumpy variety does not contain such inclusions.

116 When approaching from the open sea to the paleoshoreline, this carbonate ore passes toward a mixing
117 carbonate-oxide ore facies. The oxide-carbonate ore facie generally consists of irregular spherical masses of
118 Mn oxide varying between 0.1 and 1 cm in Mn carbonate matrix. The Mn oxide masses are about 25 % of
119 the ore. The oxide ores corroded and replacement by the carbonate matrix showed that the oxide ores formed
120 earlier than the carbonate matrix. Similar paragenesis relations (Calvert and Price 1970) are observed between
121 the cemented oxide nodules and MnCO_3 in Scotland. The carbonate masses within this facies have a similar
122 composition with the carbonate facies. The closest regions to the paleo-shoreline consist of manganese oxide
123 ores. The formation of the oxide ores in the paleo-shoreline has been still discussed that these are a deposition of
124 supergene alteration of carbonate ore or the primary oxide ore. Varentsov and Rakhmanov (1977) believe that
125 the carbonate ore and mixed carbonate-oxide ores were only primary. The oxide ores was formed as a result of
126 secondary oxidation of both carbonate and carbonate-oxide ores. The oxide ores in these areas can contain the
127 concretion or earthy masses bigger than 25 cm, sometimes with remnants of carbonate or carbonate-oxide
128 textures (Maynard, 1983). Although the well-developed concentric stratifications are observed here, smaller
129 deformed concretion is often attached to larger aggregates (Maynard, 1983). The main minerals of supergene
130 oxidation zone in Nikopol manganese deposits are: manganite, pyrolusite, todorokite, cryptomelane, birnessi-
131 birnessite, rancieite (Varentsov, 2002).

132

133 3. SAMPLES AND ANALYTICAL METHOD

134 3.1. Sampling

135 Eleven manganese oxide samples were collected from the oxide-hydroxide zones of Alexandrovsky
136 quarry areas in the Nikopol Mn deposit (Fig 2) for major oxides, trace elements, and rare earth element
137 analyses. As seen in Fig. 4, the oxide ores were sampled toward up from the bottom of the upper manganese ore
138 section. While the bottom part of the cross section generally consists of carbonate ores (with low oxide-
139 hydroxide ores) together with limestone, quartz and clay minerals, the up parts mostly consist of oxide-
140 hydroxide manganese minerals. During sampling, especially manganese oxide-hydroxide samples were
141 collected from the field for the assessment to the geochemistry of trace and rare earth elements. These samples
142 were analyzed separately to detect major oxide, trace and rare earth element contents through this section. In
143 this Fig. 4, the dark parts contains mostly manganese oxide-hydroxide ores and less limestone, quartz and clay
144 minerals, the light sections (yellow and green color) contains mostly limestone, clay minerals, quartz and less
145 manganese piece ore (Fig. 5).

146

147 **3.2. Analytical Methods**

148 Eleven Mn oxide-hydroxide samples collected from the Nikopol manganese mineralizing area were
149 broken up and after that, were milled to a 200 mesh size for both analyses of major oxides by ICP-AES, and
150 trace and rare earth elements by ICP-MS. In the analyzed samples, the error rate in repeated analyses was
151 reported to be within 5%. The major oxides were analyzed by ICP-AES, trace elements and rare earth elements
152 were analyzed by ICP-MS. All ICP-AES and ICP-MS analyses were performed by Acme Analytical
153 Laboratories in Canada. Powdered manganese samples (50 mg) were firstly digested in a mixture of
154 HCl:HNO₃:H₂O (1:1:1, v/v; 6 ml per 1.0 g of sample) for 1 hour. Then, the major oxide, trace element, and REE
155 analyses in the digested samples were determined by using ICP-AES and ICP-MS in Acme Analytical
156 Laboratory (Canada).

157 Pb isotope analysis (Pb²⁰⁸, Pb²⁰⁷, Pb²⁰⁶, and Pb²⁰⁴) was performed in manganese oxide/hydroxide
158 samples by the ICP-MS method in Acme Laboratories (Canada). These samples were solved with aqua regia
159 (3HCL + 1 HNO₃ mixture) to analyze ²⁰⁶Pb/²⁰⁴Pb, ²⁰⁷Pb/²⁰⁴Pb and ²⁰⁸Pb/²⁰⁴Pb isotope ratios. The NIST-SRM
160 981 standard was used during the Pb isotope analyses and this standard was 36.7219 for ²⁰⁸Pb/²⁰⁴Pb, 15.4916 for
161 ²⁰⁷Pb /²⁰⁴Pb value, and 16.9374 for ²⁰⁶Pb/²⁰⁴Pb value. For these values repeatability and precision in 8 hour
162 period (error ±% RSD) were calculated as ± 0.27%, ± 0.20% and ± 0.17%.

163 The corresponding values to calculate Ce, Eu and Y anomalies for each sample were normalized to
164 PAAS by using the formulas (Taylor and McLennan, 1985): Ce/Ce* = Ce_n /√[La_n *Pr_n], Eu/ Eu* = Eu_n /√[Sm_n
165 *Gd_n] and Y/Y* = Y_n/√[Dy_n *Ho_n].

166 The data were statistically analyzed using the Student Newman Keul's Procedure (SNK) (Sokal and
167 Rohlf, 1995) with SPSS 15.0 software and variance analysis (ANOVA).

168

169 **3.3. Quality Assurance**

170 Quality Assurance through the process of external auditing by recognized organizations; all facilities
171 maintain ISO registrations and accreditations. These accreditations and registrations meet the requirements of
172 the ISO standards and provide independent verification that the management systems have been implemented.
173 All BVM facilities are registered to ISO 9001 and they are pending to the Bureau Veritas corporate registration.
174 Additionally a number of analytical hubs have received ISO/IEC 17025 accreditation for specific laboratory
175 procedures.

176

177 **4. RESULTS AND DISCUSSION**

178 **4.1. Major Oxide Geochemistry**

179 Major-oxides, loss on ignition (LOI), trace elements, and rare earth element contents analysed by ICP-MS and
180 ICP-AES of 11 manganese oxide-hydroxide samples are given in Table 1. The MnO contents in the Nikopol
181 manganese deposits vary from 32.4 to 54.5 wt% with an average of 40.7%. The major oxide contents of the
182 Nikopol manganese deposits varied from 7.46 to 21.6% for SiO₂, 3.03 to 10.5% for CaO, 2.04 to 6.88% for
183 Al₂O₃, 2.91 to 5.73% for Fe₂O₃ (Table 1). Bivariate plots for n=11, of SiO₂ versus K₂O, SiO₂ versus Al₂O₃ and

184 SiO₂ versus TiO₂ have high positive correlations whereas SiO₂ versus MnO and SiO₂ versus Sr show strong
185 negative correlations. Positive correlations of SiO₂ with K₂O, Al₂O₃ and TiO₂ reflect terrigenous detritus input
186 to the depositional basin. Compared to the Binkilic (Gultekin and Balci, 2018) and Chiatura manganese
187 deposits, the Nikopol manganese deposit has higher Fe₂O₃ and MgO contents and a lower SiO₂ and Al₂O₃
188 contents for Binkilic and higher contents for Chiatura manganese oxide deposit. Nikopol manganese oxide
189 deposit chemical data are plotted on discrimination diagrams to find the genetic origin and depositional
190 environment (Fig. 5). These diagrams indicate that the Nikopol manganese oxide deposit formed as
191 hydrogenetic precipitates in shallow-marine environments. Strong linear correlations were detected in SiO₂-
192 Al₂O₃, SiO₂- TiO₂, SiO₂- K₂O, TiO₂-K₂O, MnO-P₂O₅, Al₂O₃-K₂O and Al₂O₃-TiO₂ whereas negative correlations
193 were observed in MnO-CaO, Al₂O₃-CaO, SiO₂-K₂O, and CaO-Na₂O. These major oxide correlation relations
194 show that MnO transported only to manganese ore area together with P₂O₅, not other major oxides.

195

196 **4.2. Trace Element Geochemistry**

197 The trace element contents of the Nikopol manganese oxide-hydroxide ores, together with some
198 parameters and the detection limits are given in Table 2. The total trace element concentrations in the analysed
199 ores were between 433 and 7897 ppm with a mean of 2836, whereas the average trace element content of
200 marine sediments is 760 ppm (Turekian and Wedepohl, 1961). Average concentrations for the trace elements
201 are V (95 ppm), Co (74 ppm), Ni (101 ppm), Cu (61 ppm), Sr (638 ppm), Y (18.4 ppm), Ba (1709 ppm), As
202 (19,4 ppm), U (11,7 ppm), and Zn (55,4 ppm). The Nikopol manganese ores contain more Co, Ni, Cu, Sr, Ba,
203 As, Cd and U, and lower V, Cr, Rb, Zr, Nb, Hf, Th, Pb and Zn compared to Post Archean Australian Shale
204 (PAAS) (Taylor and McLennan, 1985) (Fig. 6). While the Sr and Ba from the LILE elements are slightly
205 enriched, Zr, Hf, Nb and Rb is strongly depleted in compared to PAAS (Fig 6). The PAAS-normalized
206 ferromanganese-hosted trace elements (Co, Ni and Cu) showed strong enrichments together with As, Ba, and U,
207 except for Pb, Zn, V and Cr (Fig. 6). For the HFSE (Y, Zr, Hf, Nb, U and Th), Nb, Zr, Hf, and Th are highly
208 depleted, except for Sr, Y and U. The average Mn/Fe, Co/Zn, Co/Ni, and Zr/Hf ratios in the Nikopol
209 manganese oxide ores are 25, 0.54, 1.15, and 57, respectively (Table 2).

210 Discrimination diagrams for Mn-Fe-(Ni + Co + Cu)x10 (Bonatti et al., 1972; Crerar et al., 1982) and
211 Zn-Ni-Co (Choi and Hariya, 1992) trace element concentrations in the Nikopol manganese oxide ores indicate
212 the mostly hydrothermal+diagenetic and hydrogenetic origins (Fig. 5).

213 The major oxide and trace element contents for different type manganese deposits in the world are given
214 in Table 3. These contents of the Nikopol manganese deposit are similar with those of the Hazara, Binkilic,
215 Elazig and Chiatura Mn deposits in Turkey (Shah and Moon, 2007; Gultekin and Balci, 2018; Sasmaz et al.,
216 2014) (Table 3). The ratios between Mn and Fe are defined as Mn:Fe = 16.76 (5.38 to 58.31) for the Binkilic
217 sedimentary manganese deposit, Turkey; Mn:Fe = 0.63 for SEDEX manganese deposits around Elazig, Turkey;
218 Mn:Fe 0.1-10 for SEDEX deposits; Mn:Fe = 1 for a hydrogenous origin and Mn:Fe <1 for a lacustrine
219 environment. The Mn:Fe ratios of Nikopol manganese oxide-hydroxide ores vary from between 6.2 and 47
220 (average = 25) (Table 3) and have similar values with Binkilic sedimentary manganese deposits (Gultekin and

221 Balci, 2018).

222 The Zr/Hf ratios vary from 33 to 83 with an average of 57 (Table 2). The Nb/Ta ratios range from 2,3 to
223 8.6 with a mean of 4.13 (Table 2). Fig. 8 shows that the Zr/Hf ratios are similar with North Atlantic Deep Water,
224 Atlantic Fe-Mn crusts and Surface Pacific Fe-Mn crusts and but, the Nb/Ta ratios are lower than for North
225 Atlantic, Pacific, and Southern Ocean Deep Waters (Godfrey et al., 1996, 2009; Firdaus et al., 2011; Schmidt et
226 al., 2014; Censi et al., 2007; 2010; 2017) (Fig 8). The HFSE enrichments in hydrogenetic oxides result from
227 absorption from sea water (Firdaus et al., 2011; Schmidt et al., 2014; Censi et al., 2018; 2019). This also shows
228 that the low Zr/Hf and Nb/Ta ratios in the studied manganese oxide ores indicate a low HFSE content in the
229 seawater during the formation of these manganese oxide-hydroxide ores.

230

231

232 **4.3. Rare Earth Element Geochemistry**

233 Table 4 represents the REE+Y concentrations of the Nikopol manganese oxide-hydroxide ores. The
234 average Σ REE concentrations change between 60 ppm and 197 ppm with an average of 108 ppm (Table 4). The
235 Y concentrations vary from 9.1 to 47.1 with average of 18.2 ppm. Shale-normalised patterns of the studied
236 manganese oxide-hydroxide samples (relative to PAAS, Post Archean Australian Shale; Taylor and McLennan,
237 1995) are reported in Fig 8. The PAAS-normalized REE +Y patterns of these samples followed similar trends to
238 each other and are characterized by a general increase in normalized concentrations along the series, from light
239 REE to heavy REE (Fig. 8). The average REE sequence in the PAAS-normalized REE pattern for the Nikopol
240 manganese oxide-hydroxide ores is as follows: MREE (3,59) > HREE (3,04) > LREE (2,13 (Fig. 8). The
241 La_n/Yb_n ratios are used to determine the enrichment trends for light and heavy REE contents. The La_n/Yb_n ratios
242 of the Nikopol manganese oxide-hydroxide ores ranged between 0.68 and 1.06 with a mean of 0.86, verifying
243 the MREE and HREE enrichments.

244 Cerium is probably the most efficient element of the REE series to use as a discriminating feature for
245 Fe-Mn deposits. In fact, Ce readily oxidizes and is continuously and irreversibly removed from seawater at the
246 surface of Mn oxides (Takahashi et al., 2007), and therefore positive Ce anomalies in Fe-Mn oxide deposits are
247 considered typical of hydrogenetic deposition. Due to differences in the kinetics among the different Fe-Mn
248 deposits and irreversible Ce uptake from sea water, Ce will be most enriched in hydrogenetic deposits, lower in
249 diagenetic deposits, and lower yet in hydrothermal deposits (Josso et al., 2017). The Ce/Ce* and Eu/Eu* ratios
250 have been used as an indicator of redox state to obtain the physicochemical characteristics of hydrothermal
251 fluids or the depositional environment including fO_2 , pH, and temperature (Bau and Möller, 1992; Bau, 1996).
252 The Ce/Ce* values of manganese oxide-hydroxide ores collected from the study area vary from 0.88 to 1.43,
253 with the mean of 1.16, which are positive Ce anomalies ($Ce/Ce^* = Ce_n/\sqrt{[La_n*Pr_n]}$), except for 3 samples,
254 indicating that ore-forming rocks were primarily marine chemical or biogenic deposit (Table 4). Under seawater
255 Eh and pH condition, Ce is primarily Ce^{4+} , its solubility very low, and thus it is not easy to remain dissolved in
256 sea water. It precipitates as Ce^{4+} (CeO_4), causing strong depletion Ce in sea water. The Ce concentrations in the
257 oxide ore are higher than in the primary carbonate ore, because of the redox potential of those two

258 environments. For example, the seawater shows a strong negative Ce anomaly which is mirrored by a positive
259 anomaly in hydrogenetic ferromanganese crusts and nodules (Elderfield, 1988). However, all the manganese
260 oxide samples had Ce values close to 1 indicative of rapid deposition of the oxide ores and typically lack of
261 enrichment of REE in carbonates. Ce can occur in both the +3 and +4 in oxidation states. Ce (III) in the
262 presence of oxygen is oxidised partially to Ce (IV) on the surface of Mn oxides, where it no longer joins in
263 desorption reactions, leaving seawater depleted in Ce relative to other trivalent REEs. This Ce fractionation only
264 occurs under oxic conditions (German and Elderfield, 1990; German et al., 1991). Negative Ce anomalies can
265 occur in the well-oxygenated modern oceans and indicates rapid deposition of the oxides, not leaving time for
266 the surface oxidation of the Ce (Tostevin et al., 2016). Mn is generally accepted as the main carrier phase for Ce
267 (Bau et al., 2014). Since both Mn and Ce have a high reduction potential, the formation of Ce-enriched Mn
268 oxides needs high dissolved oxygen concentrations based on redox proxies trace elements in the Fe-C-S
269 systems. Local positive Ce anomalies in some modern dissolved Mn-rich develops beneath the Mn (IV/II) redox
270 cline (De Carlo and Green, 2002; De Baar et al., 1988; Bau et al., 1997). This positive Ce anomaly has been
271 reported to occur in late Ediacaran carbonates (Mazumdar et al., 2003), cherts and Fe formations from the
272 Palaeoproterozoic (Slack et al., 2007). This is more likely to inheritance from mineralization of a Mn oxide-
273 hydroxide. Ce anomalies are used as a common redox proxy to speculate on the oxygenation of the marine
274 environment during the Phanerozoic or Precambrian anoxic events (Liu et al., 1988; Bodin et al., 2013; Riding
275 et al., 2014; Tostevin et al., 2016).

276 Eu anomalies of the manganese oxide-hydroxide ores in the Nikopol are close to 1 ($\text{Eu}/\text{Eu}^* = \text{Eu}_n$
277 $/\sqrt{[\text{Sm}_n * \text{Gd}_n]}$), with a range of 0.68 to 1.12 (mean: 0.96) (Table 3). Six samples have slightly positive Eu
278 anomaly higher than 1, five samples have slightly negative Eu anomaly because of lower than 1. The positive
279 Eu anomalies indicate the existence of Eu^{2+} during deposition and low oxygen fugacity conditions of the
280 hydrothermal solutions. The manganese precipitated from fluids with decreasing temperature or increasing $f\text{O}_2$
281 or alternatively co-precipitated together with Eu-enriched minerals. Eu anomalies can be related to a few
282 factors, such as increases in pH and $f\text{O}_2$ or decrease in temperature (Ehya, 2012; Deng et al., 2014). Positive Eu
283 anomaly in a PAAS-normalized REE pattern may due to hydrothermal fluids involved in the mineralization
284 (Abedini and Calagari 2015; Tobia 2018). Limestone is generally deposited in a shallow-marine carbonate
285 environment; therefore, local feldspar enrichment in diagenetic environments may also lead to positive Eu
286 anomaly (Roy et al., 2018). Schwinn and Markl (2005) suggested that the reduction of Eu^{3+} to Eu^{2+} occurred at
287 high temperatures which resulted in Eu-enrichment in the minerals relative to the fluids.

288 Common ternary diagrams do not clearly differentiate Fe-Mn deposits formed by mixed genetic
289 processes (Josso et al., 2017). There are different methods to date which allow us to find out their origins of the
290 Fe-Mn samples based on their trace element compositions (Bau et al., 2014, Josso et al., 2017). The Ce (Ce,
291 Ce/Ce^*), Y, Ho, Nd, and Zr concentrations is used as a main tool for investigating the genesis of manganese
292 oxide samples (Bau et al., 2014, Josso et al., 2017). Our samples were plotted on the diagrams along with
293 several typical examples of diagenetic, hydrogenetic, and hydrothermal Fe-Mn deposits (Zeng et al., 2012; Bau
294 et al., 2014; Josso et al., 2017). Both $(\text{Ce}/\text{Ce}^*)_n$ vs Nd and Ce vs $(\text{Co}+\text{Ni}+\text{Cu})/1000$ diagrams in Fig. 9a,b

295 showed that the Nikopol samples cover similar areas with Baturin (2011) and Vereshchagin et al.
296 (2019)'s samples. Although diagenetic Fe - Mn nodules usually show negative Ce anomaly (Fig 9a), the Nd
297 concentrations in diagenetic manganese have higher concentrations than those of hydrothermal manganese and
298 vary between 10 and 100 ppm (Bau et al., 2014; Vereshchagin et al., 2019). The Ce vs Zr diagram for the
299 Nikopol samples indicated that our samples overlapped in an area between diagenetic and hydrothermal
300 proposed by Bau et al. (2014) (Fig 9c). Ce/Ce^*_n vs $(Y/Ho)_n$ diagram showed that our samples mostly located
301 within the area of hydrothermal manganese deposits (Fig 9d). The $(Y/Ho)_n$ ratio shows decoupling of the
302 geochemical twins Y and Ho, which produces Y anomalies within REY patterns due to very similar ionic radius
303 to Ho^{3+} , Y^{3+} can be inserted into REE patterns between isoivalent Dy^{3+} and Ho^{3+} (Bau, 1996). This decoupling
304 results from preferential scavenging of Ho relative to Y on metal oxide surfaces due to lower stabilities of Y
305 surface complexes (Bau, 1996; Bau, 1999). The Y/Ho values of the manganese oxide-hydroxide ores in the
306 study area vary from 23 to 30, with an average of 26. The REY pattern in anoxic Mediterranean seawater has a
307 negative Ce and positive Y anomalies. The change to a positive anomaly in M-3400 from a negative Ce
308 anomaly in sample M-3200 strongly suggests that in the Tyro sub-basin, similar to the situation in the Bannock
309 sub-basin, Y and REE are involved in the redox-cycling of Mn and Fe (Bau et al., 1997).

310 The Y concentrations in the Nikopol manganese ores vary from 9,1 to 47,1 ppm, with an average of
311 18.2 ppm (Table 4). Nikopol manganese oxide-hydroxide samples show negative Y anomalies, except for three
312 samples ($Y/Y^* = Y_n/\sqrt{(Dy_n * Ho_n)}$) between 0.75 and 1.12 with a mean of 0.93 (Table 4). The anoxic water
313 sample shows a REY pattern with considerably less HREE enrichment and less positive Y anomaly in compared
314 to the oxic water. However, the most remarkable variation is the presence of a positive Ce anomaly in the
315 anoxic brine (Bau et al., 1997). These data also show that in environments where manganese deposits are
316 formed, oxic environments from time to time and anoxic environments prevail. Chen et al. (2018) studied the
317 REY geochemistry of the ferromanganese oxides on the eastern flank of the Gagua Ridge collected from a water
318 depth of 4071m. According these results, the REY data, which are normalized to PAAS, exhibited flat patterns
319 with positive Ce anomalies and negative Y anomalies as Nikopol manganese oxide-hydroxide ores.

320 The Cape Vani (Milos Island, Greece) Mn-oxide and barite deposit shows the three-dimensional
321 characteristics of a shallow-water hydrothermal system between Mn-oxide ores and barite deposits (Hein et al.,
322 1999, 2000). The hydrothermal fluid was predominantly enriched seawater in metals leached from the basement
323 rocks. The hydrothermal solutions were supported by convection driven by heating from a magma source. Mn-
324 oxide mineralization and barite precipitation were syngenetic. We envision that fluids from a similar
325 hydrothermal system contributed to the formation of Chiatura Mn-oxide deposits that combined with the
326 production of Mn-oxides from diagenetic processes, thereby creating a mixed origin ore deposit. It is observed
327 that similar barite and pyrite formations occur with the continuation of Kockale manganese-oxide ore section in
328 Maden Complex (Sasmaz et al., 2014).

329

330 **4.4. Pb Isotope Geochemistry**

331 The Pb isotope ratios of Nikopol manganese oxide-hydroxide ores are 18.98 for $^{206}\text{Pb}/^{204}\text{Pb}$, 15.68 for
332 $^{207}\text{Pb}/^{204}\text{Pb}$ and 39.39 for $^{208}\text{Pb}/^{204}\text{Pb}$ isotopes (Table 4). According to Wang et al. (2014), The Pb isotope studies
333 in the study area show that Pb in the manganese oxide ores originated from upper crust materials. The
334 $^{207}\text{Pb}/^{204}\text{Pb}$ isotope ratios vary from 15.64 to 15.73. These values showed that the Nikopol manganese ores were
335 mostly sourced from fluids or metals with upper crust origin (Zartman and Doe, 1981). Pb isotopes values and
336 their potential sources that may support to the seawater Pb isotope composition recorded by Fe-Mn crusts are
337 given in Fig. 10. These ratios indicate that Pb isotope data covered similar areas with the Atlantic crust and
338 pelagic sediments. (Fig 10a,b). These are hydrothermal lead, derived from MORB, continental sources as shown
339 by riverine particulates, island arcs, and young continental margins (von Blanckenburg et al., 1996). The highly
340 radiogenic Pb isotope values in the North Atlantic have been explained by incongruent weathering processes on
341 the old cratonic landmasses of Greenland and northern Canada (von Blanckenburg and Nagler, 2001). The Pb
342 isotope composition of the shallowest crust that grew within the present-day Mediterranean Outflow Water does
343 not show significant Pb isotope changes indicating that it was controlled by the same Pb sources throughout the
344 past 15 Ma. Time series of Pb isotope composition was measured on three ferromanganese crusts recording the
345 evolution of NE Atlantic water masses over the past 15 Ma. The crusts are observed along a depth profile
346 (~700–4600 m) comprising the present-day depths of NE Atlantic Deep Water and Mediterranean Outflow
347 Water. The Pb isotope evolution during the Pliocene-Pleistocene can generally be explained by mixing between
348 two end-members corresponding to NE Atlantic Deep Water and Mediterranean Outflow Water, but Muiños et
349 al. (2008) reported that external sources such as Saharan dust can play an important role in the composition
350 change of waters in this region. Andrieu et al. (1998) investigated that Pb isotope analyses on the basalts and
351 sulfides from the Trans-Atlantic Geotraverse (TAG) hydrothermal site on slow-spreading Mid-Atlantic Ridge
352 (Fig. 10c,d). These data show that the Pb isotope ratios of TAG sulphides reflect the average isotope
353 composition of the upper part of the ocean crust affected by the large-scale hydrothermal fluid circulation, and
354 the sulphides of the Pb isotopic compositions of hydrothermal aeration fluids recorded recently and in the
355 ancient period remain active throughout the active range of a main hydrothermal vent area such as TAG
356 (Andrieu et al., 1998). Fig 10c,d shows that Pb isotope data of Nikopol manganese oxide ores covered the same
357 areas with terrigenous sediments, Mn nodules and pelagic and biogenic sediments.

358 5. CONCLUSION

359 The Nikopol manganese deposit located in the Eastern Paratethys basin the Nikopol at the southeast of
360 Ukraine is one of the largest manganese deposits of metallurgical manganese in the world among the
361 sedimentary manganese deposits. The Nikopol Oligocene basin observed between the Azov crystalline massif
362 and the Ukrainian crystalline shield. Oligocene marine basin is a single basin as structural, stratigraphic, and
363 genetic. All separate ore-bearing parts in this basin are parts of a same system in Oligocene basin. The Nikopol
364 Oligocene basin consists of two structural stages, Precambrian crystalline basement rocks and sedimentary
365 cover rocks from the Cretaceous to Quaternary. Nikopol Ore horizon is traced in a thickness varying from
366 several cm to 4.5 m and a single stratum from the west to the eastwards to about 250 km (Fig. 11). Nikopol

367 manganese ore horizon was separated to three different units; carbonate ore, mixed carbonate-oxide ore, and
368 oxide ore (Fig. 11). As it approaches the paleoshoreline from the open sea, it first shows mixed ores and then
369 completely oxide ores. The oxide ores formed earlier than the carbonate matrix and therefore, they were
370 corroded and filled by the carbonate matrix (Fig. 11). The oxide ores can contain the concretion or earthy
371 masses bigger than 25 cm, sometimes with remnants of carbonate or carbonate-oxide textures. The main
372 minerals of the oxide zone are: manganite, pyrolusite, and psilomelano. The principal carbonate minerals are
373 manganocalcite and rhodocrosite. MnO contents of the Nikopol manganese oxide-hydroxide deposit have the
374 highest values, except for the Binkilic, Koryu and Hinode deposits. Fe₂O₃ contents have similar values with
375 Chiatura and Binkilic manganese. Trace element contents of the Nikopol deposit are higher values than in most
376 of these other manganese deposits, and but, lower than in the Chiatura, Binkilic and Elazig manganese deposits
377 especially in terms of Co, Ni, Cu, Sr, Ba and As. The ΣREE values of the Nikopol manganese oxide ores change
378 between 60 ppm and 197 ppm with an average of 108 ppm. The Y concentrations vary from 9.1 to 47.1 with
379 average of 18.2 ppm. The PAAS-normalized REE +Y patterns of these samples followed similar trends to each
380 other and are characterised by a general increase in normalised concentrations along the series, from light REE
381 to heavy REE (Fig. 8). The average REE sequence in the PAAS-normalized REE pattern for the Nikopol
382 manganese oxide-hydroxide ores is as follows: MREE (3,59) > HREE (3,04) > LREE (2,13). The La_n/Yb_n ratios
383 of the Nikopol manganese oxide-hydroxide ores ranged between 0.68 and 1.06 with a mean of 0.86, verifying
384 the MREE and HREE enrichments. In addition, when compared to PAAS-normalized REY pattern of different
385 environments reported by Bau et al. (1997), the Nikopol manganese oxide ores have similar pattern to
386 hydrogenetic Fe-Mn nodules (Fig. 11). The Ce/Ce* values of manganese oxide-hydroxide ores collected from
387 the study area vary from 0.88 to 1.43, with the mean of 1.16. Most of manganese samples have positive Ce
388 anomalies except for a few samples, indicating that ore-forming rocks were primarily marine chemical or
389 biogenic deposit. Local positive Ce anomalies in some modern dissolved Mn-rich develops beneath the Mn
390 (IV/II) redox cline (De Carlo and Green, 2002; De Baar et al., 1988; Bau et al., 1997). This positive Ce
391 anomaly has been reported to occur in late Ediacaran carbonates (Mazumdar et al., 2003), cherts and Fe
392 formations from the Palaeoproterozoic (Slack et al., 2007). This is more likely to inheritance from
393 mineralization of a Mn oxide-hydroxide. Ce anomalies are used as a common redox proxy to speculate on the
394 oxygenation of the marine environment during the Phanerozoic or Precambrian anoxic events (Liu et al., 1988;
395 Bodin et al., 2013; Riding et al., 2014; Tostevin et al., 2016). All these data indicate that the Nikopol manganese
396 deposit formed in an environment where increase/decreases in *f*O₂ and pH or increase in temperature in
397 compared to similar environments, low-oxygen fugacity in source of the hydrothermal fluids, volcanogenic
398 input or hydrothermal contributions to seawater, and high Co, Ni, Cu, Sr, Ba and As and low V, Rb, Nb, Hf, U,
399 Th, Pb and Zn values. Maynard (1983) reported that Oxide and nodules in the Nikopol ores had more Ni, Cu,
400 Co, V concentrations than in mixed and carbonate ores in Nikopol manganese deposit. This indicates that the
401 hydrothermal fluids played an important role in the formation of manganese mineralization, especially during
402 the formation of the oxide ores. As indicated by Bolton and Frakes (1985), manganese, which resulted from the
403 decomposition of regional rocks with average shell abundance values, was concentrated in a dissolved form in

404 an oxygen depleted basin during marine transgression. Manganese initially precipitated as oxides and
405 hydroxides ahead of the landward migrating oxidation/reduction interface is largely diagenetically remobilized
406 and eventually concentrated at the shoreline edge where it is precipitated as oxides. Manganese ores were
407 deposited during "transgression" in shallow marine environments. All data show that the oxide-hydroxide ores
408 in Nikopol manganese deposit formed in the upper zones and the mixed and carbonate ores formed in deeper
409 parts of the sea.

410 All geochemical data show that the Nikopol manganese-oxide ores formed rapidly within oxic/suboxic
411 seawater as reflected by the Ce anomalies close to 1. The mixed oxide and carbonate ores formed at deeper-
412 water depths compared to the oxide-hydroxide ores in the Nikopol region. Also, our results point out that the
413 metals were transported from both terrestrial sources (Pb isotopic data) and a hydrothermal source in deeper
414 water (chemical discrimination diagrams). The metals associated with the Mn-oxide ores likely formed
415 syngenetically through microbially mediated mineralization at water depths deeper than the area where the
416 carbonate-ore deposits formed.

417 **Acknowledgements**

418 This work was financially supported by the Firat University (MF.18.49) for financial supports. I would
419 like to thank to POKROV GOK Mining and Processing Plant (Nikopol) and Chief Geologists Sergey
420 Svietchichnyi and Senior Geologist Konstantin Gogolev (Institute of Geochemistry, Kiev) for helpings and
421 supports during field study in Nikopol.

422 **References**

- 424 Abedini, A., Calagari, A.A. 2015. Rare earth element geochemistry of the Upper Permian limestone: the Kanigorgeh
425 mining district, NW Iran. *Turk J Earth Sci* 24:365–382.
- 426 Akgul, B. (2015) Geochemical associations between fluorite mineralization and A-type shoshonitic magmatism in the
427 Keban–Elazig Area, East Anatolia, Turkey. *J. Afr. Earth Sci.* 111, 222–230.
- 428 Andrieu, A.S., Honnorez, J., Lancelot, J., 1998. Lead isotope compositions of the TAG mineralization, Mid-Atlantic Ridge,
429 26°08'N. In: Herzig, P.M., Humphris, S.E., Miller, D.J., Zierenberg, R.A. (Eds.), *Proceedings of the Ocean Drilling*
430 *Program, Scientific Results*.
- 431 Baturin, G.N., 2009. Geochemistry of ferromanganese nodules in the Gulf of Finland, Baltic Sea. *Lith. Miner. Resour.* 44
432 (5), 411–426.
- 433 Baturin, G.N., Dubinchuk, V.T., 2009. Composition of ferromanganese nodules from Riga Bay (Baltic Sea). *Oceanology*
434 49 (1), 111–120.
- 435 Baturin, G.N., 2011. Variations in the composition of ferromanganese concretions of the Kara Sea. *Okeanologiya* 51 (1),
436 153–161 (in Russian).
- 437 Bau M. 1996. Controls on the fractionation of isovalent trace elements in magmatic and aqueous systems: evidence from
438 Y/Ho, Zr/Hf, and lanthanide tetrad effect. *Contrib. Mineral. Petrol.* 123, 323–333
- 439 Bau, M., Möller, P., 1992. Rare-earth element fractionation in metamorphogenic hydrothermal calcite, magnesite and
440 siderite. *Minerol. Petrol.* 45, 231–246
- 441 Bau, M., Dulski, P., 1996. Distribution of yttrium and rare-earth elements in the Penge and Kuruman iron-formations,
442 Transvaal Supergroup, South Africa. *Precambrian Res.* 79, 37–55.

- 443 Bau, M., Möller, P., Dulski, P., 1997. Yttrium and lanthanides in eastern Mediterranean seawater and their fractionation
444 during redox-cycling. *Mar. Chem.* 56, 123–131.
- 445 Bau, M., 1999. Scavenging of dissolved yttrium and rare earths by precipitating iron oxyhydroxide: experimental evidence
446 for Ce oxidation, Y-Ho fractionation, and lanthanide tetrad effect. *Geochim. Cosmochim. Acta* 63, 67–77.
- 447 Bau, M., Schmidt, K., Koschinsky, A., Hein, J.R., Kuhn, T., Usui, A., 2014. Discriminating between different genetic types
448 of marine ferro-manganese crusts and nodules based on rare earth elements and yttrium. *Chem. Geol.* 381, 1–9.
- 449 Ben Othman, D., White, W.M., Patchett, J. 1989. The geochemistry of marine sediments, island arc magma genesis and
450 crust-mantle recycling. *Earth Planet. Sci. Lett.* 94, 1–21.
- 451 Bodin, S., Godet, A., Westermann, S., Föllmi, K.B., 2013. Secular change in Northwestern Tethyan water-mass
452 oxygenation during the late Hauterivian–early Aptian. *Earth Planet. Sci. Lett.* 374, 121–131.
- 453 Bolton, B.R., Frakes, L.A. 1985. Geology and genesis of manganese oolite, Chiatara, Georgia, U.S.S.R. *Geol Soc Am Bull*
454 96, 1398–1406.
- 455 Bonatti, E., Kraemer, T., Rydel, H., 1972. Classification and genesis of submarine iron–manganese deposits. In: Horn, D.R.
456 (Ed.), *Ferromanganese Deposits on the Ocean Floor*, Washington, D. C., Natl. Sci. Found, pp. 149–166.
- 457 Censi, P., Sprovieri, M., Larocca, D., Aricò, P., Saiano, F., Mazzola, S., Ferla, P., 2007. Alteration effects of volcanic ash
458 in seawater: Anomalous Y/Ho ratios in coastal waters of the Central Mediterranean Sea. *Geochem. Cosmochim.*
459 *Acta* 71 (22), 5405–5422.
- 460 Censi, P., Randazzo, L.A., Zuddas, P., Saiano, F., Aricò, P., Andò, S., 2010. Trace element behaviour in seawater during
461 Etna's pyroclastic activity in 2001: concurrent effects of nutrients and formation of alteration minerals. *J. Volcanol.*
462 *Geotherm. Res.* 193 (1–2), 106–116.
- 463 Censi, P., Inguaggiato, C., Chiavetta, S., Schembri, C., Sposito, F., Censi, V., Zuddas, P., 2017. The behaviour of
464 zirconium, hafnium and rare earth elements during the crystallisation of halite and other salt minerals. *Chem. Geol.*
465 453, 80–91.
- 466 Censi, P., Sposito, F., Inguaggiato, C., Zuddas, P., Inguaggiato, S., Venturi, M., 2018. Zr, Hf and REE distribution in river
467 water under different ionic strength conditions. *Sci. Total Environ.* 645, 837–853.
- 468 Censi, P., Raso, M., Saiano, F., Zuddas, P., Oliveri, E. 2019. Zr/Hf ratio and REE behaviour: A coupled indication of
469 lithogenic input in marginal basins and deep-sea brines. *Deep-Sea Res. Part II* 164, 216–223.
- 470 Chakhmouradian, A.R., Wall, F., 2012. Rare earth elements: minerals, mines, magnets (and more). *Elements* 8, 333–342
- 471 Chen, S., Yin, X.B., Wang, X.Y., Huang, X., Ma, Y., Guo, K., Zeng, Z.G. 2018. The geochemistry and formation of
472 ferromanganese oxides on the eastern flank of the Gagua Ridge. *Ore Geol. Rev.*, 95, 118–130
- 473 Choi, J.H., Hariya, Y., 1992. Geochemistry and depositional environment of Mn oxide deposits in the Tokora Belt,
474 northeastern Hokkaido, Japan. *Econ. Geol.* 87, 1265–1274.
- 475 Crerar, D.A., Namson, J., Chyi, M.S., Williams, L., Feigenson, M.D., 1982. Manganiferous cherts of the Franciscan
476 assemblage: I. General geology, ancient and modern analogues, and implications for the hydrothermal convection at
477 oceanic spreading centers. *Econ. Geol.* 77, 519–540
- 478 De Baar, H.J., German, C.R., Elderfield, H., van Gaans, P., 1988. Rare earth element distributions in anoxic waters of the
479 Cariaco Trench. *Geochim. Cosmochim. Acta* 52, 1203–1219
- 480 De Carlo, E.H., Green, W.J., 2002. Rare earth elements in the water column of Lake Vanda, McMurdo Dry Valleys,
481 Antarctica. *Geochim. Cosmochim. Acta* 66, 1323–1333

482 Deng, X.H., Chen, Y.J., Yao, J.M., Bagas, L., Tang, H.S., 2014. Fluorite REE-Y (REY) geochemistry of the ca. 850 Ma
483 Tumen molybdenite-fluorite deposit, eastern Qinling, China: constraints on ore genesis. *Ore Geol. Rev.* 63, 532–543

484 Dill, H.G., Hansen, B.T., Weber, B., 2011. REE contents, REE minerals and Sm/Nd isotopes of granite- and unconformity-
485 related fluorite mineralization at the western edge of the Bohemian massif: with special reference to the Nabburg-
486 Wölsendorf District, SE Germany. *Ore Geol. Rev.* 40, 132–148.

487 Dosso, L., Hanan, B.B., Bougault, H., Schilling, J.G., and Joron, J.-L., 1991. Sr-Nd-Pb geochemical morphology between
488 10° and 17° N on the Mid-Atlantic Ridge: a new MORB isotope signature. *Earth Planet. Sci. Lett.*, 106:29-43.

489 Dosso, L., Bougault, H., and Joron, J.L., 1993. Geochemical morphology of the North Atlantic Ridge, 10°-24°N: trace
490 element-isotope complementarity. *Earth Planet. Sci. Lett.*, 120:443-462.

491 Dubinin, A.V., 2006. Rare Earth Elements in the Ocean. Nauka, Moscow (in Russian with English abstract).

492 Ehya, F., 2012. Variation of mineralizing fluids and fractionation of REE during the emplacement of the vein-type fluorite
493 deposit at Bozijan, Markazi Province, Iran. *J. Geochem. Explor.* 112, 93–106.

494 Elderfield, H. 1988. The oceanic chemistry of the rare-earth elements. *Phil. Transac. Roy. Soc. London* A325, 105–126.

495 Firdaus, M.L., Minami, T., Norisuye, K., Sohrin, Y. 2011. Strong elemental fractionation of Zr–Hf and Nb–Ta across the
496 Pacific Ocean. *Nat. Geosci.* 4, 227–230.

497 German, C.R., Elderfield, H., 1990. Application of the Ce anomaly as a paleoredox indicator: the ground rules.
498 *Paleoceanography* 5, 823.

499 German, C.R., Holliday, B.P., Elderfield, H., 1991. Redox cycling of rare earth elements in the suboxic zone of the Black
500 Sea. *Geochim. Cosmochim. Acta* 55, 3553–3558.

501 Godfrey, L.V., Mills, R., Elderfield, H., and Gurvich, E., 1994. Lead behaviour at TAG hydrothermal vent field, 26°N,
502 Mid-Atlantic ridge. *Mar. Chem.*, 46:237-254.

503 Godfrey L.V., White, W.M., Salters, V J.M. 1996. Dissolved zirconium and hafnium distributions across a shelf break in
504 the northeastern Atlantic Ocean. *Geochim. Cosmochim. Acta* 60, 3995–4006.

505 Godfrey, L.V., Zimmermann, B., Lee, D.C., King, R.L., Vervoort, J.D., Sherrell, R.M., Halliday, A.N. 2009. Hafnium and
506 neodymium isotope variations in NE Atlantic seawater. *Geochem. Geophys. Geosyst.* 10, 1-13.

507 Gultekin AH. 1998. Mineralogical and chemical doses are used to determine the origins of manganese deposits. *Geol Eng*
508 50: 39-46.

509 Gultekin, A.H., Balci, N. 2018. Geochemical Characteristics of Sedimentary Manganese Deposit of Binkılıç, Trache Basin,
510 Turkey. *J Geol Geophys* 7/3, 336.

511 Hart, S.R., 1984. A large-scale isotope anomaly in the Southern Hemisphere mantle. *Nature*, 309:753-757.

512 Hein, J.R., Koschinsky, A., Halbach, P., Manheim, F.T., Bau, M., Kang, J.-K., Lubik, N., 1997. Iron and manganese oxide
513 mineralization in the Pacific. In: Nicholson, K., Hein, J.R., Bühn, B., Dasgupta, S. (Eds.), *Manganese*
514 *Mineralization: Geochemistry and Mineralogy of Terrestrial and Marine Deposits.* 123–138.

515 Hein, J.R., Bolton, B. 1994. Formation of the Chiatura and Nikopol manganese carbonate ores, Georgia and Ukraine.
516 Abstracts, Fermor Lecture Meeting, The Geological Society of London, 26-27 September, 1994, London, UK, p. 12.

517 Hein, J.R., Mizell, K., Koschinsky, A., Conrad, T.A., 2013. Deep-ocean mineral deposits as a source of critical metals for
518 high- and green-technology applications: comparison with land-based resources. *Ore Geol. Rev.* 51, 1–14.

519 Hein, J.R., Koschinsky, A., 2014. Deep-ocean ferromanganese crusts and nodules. In: Holland, H.D., Turekian, K.K.
520 (Eds.), *Treatise on Geochemistry*, second edition 13. Oxford, Elsevier 273–291.

- 521 Hein, J.R., Spinardi, F., Okamoto, N., Mizell, K., Thorburn, D., Tawake, A., 2015. Critical metals in manganese nodules
522 from the Cook Islands EEZ, abundances and distributions. *Ore Geol. Rev.* 68, 97–116.
- 523 Hein, J.R., Konstantinova, N., Mikesell, M., Mizell, K., Fitzsimmons, J.N., Lam, P.J., Jensen, L.T., Xiang, Y.,
524 Gartman, A., Cherkashov, G., Hutchinson, D.R., Till, C.P. 2017. Arctic deep water ferromanganese-oxide deposits
525 reflect the unique characteristics of the Arctic Ocean. *Geochem. Geophys. Geosyst.*, 18, 3771-3800.
- 526 Ito, E., White, W.M., Göpel, C. 1987. The O, Sr, Nd and Pb isotope geochemistry of MORB. *Chem. Geol.*, 62, 157-176.
- 527 Josso, P., Pelleter, E., Pourret, O., Fouquet, Y., Etoubleau, J., Cheron, S., Bollinger, C., 2017. A new discrimination
528 scheme for oceanic ferromanganese deposits using high field strength and rare earth elements. *Ore Geol. Rev.* 87, 3–
529 15.
- 530 Koç, S., Özmen, Ö., Öksüz, N., 2000. Kasımağa (Keskin-Kırıkkale) mangan oksit cevherleşmesinin oluşum ortamını
531 tanımlayan jeokimyasal özellikler. *MTA Dergisi* 122, 107–118 (in Turkish).
- 532 Konstantinova, N., Cherkashov, G., Hein, J. R., Mirão, J., Dias, L., Madureira, P., & Kuznetsov, V., 2017. Composition
533 and characteristics of the ferromanganese crusts from the western Arctic Ocean. *Ore Geology Reviews*, 87, 88–99.
- 534 Kuleshov, V. 2017. *Isotope Geochemistry. The origin and formation of manganese rocks and ores.* Elsevier Amsterdam,
535 Netherlands 427p.
- 536 Lavelle, J.W., Cowen, J.P., Massoth, G.J., 1992. A model for deposition of hydrothermal manganese near mid-ocean ridge
537 crests. *Journal of Geophysical Research* 97, 7413 – 7427.
- 538 Lilley, M.D., Feely, R.A., Trefry, J.H., 1995. Chemical and biochemical transformations in hydrothermal plumes. In:
539 Humphris, S.E., Zierenberg, R.A., Mullineaux, L.S., Thomson, R.E. (Eds.), *Seafloor Hydrothermal Systems:*
540 *Physical, Chemical, Biological and Geological Interactions.* Am. Geophys. Union, Geophys. Monogr., 91, 369 –
541 391.
- 542 Liu, Y.-G., Miah, M., Schmitt, R., 1988. Cerium: a chemical tracer for paleo-oceanic redox conditions. *Geochim.*
543 *Cosmochim. Acta* 52, 1361–1371.
- 544 Maynard, J. B., 1983. *Geochemistry of sedimentary ore deposits: New York, Heidelberg, Berlin, Springer-Verlag*, p. 121-
545 144.
- 546 Mazumdar, A., Tanaka, K., Takahashi, T., Kawabe, I. 2003. Characteristics of rare earth element abundances in shallow
547 marine continental platform carbonates of Late Neoproterozoic successions from India. *Geochem. J.* 37, 277–289
- 548 McLennan, S.M., 1989. Rare earth elements in sedimentary rocks; influence of provenance and sedimentary processes.
549 *Rev. Mineral. Geochem.* 21, 169–200.
- 550 Mills, R., Elderfield, H., and Thompson, J., 1993. A dual origin for the hydrothermal component in a metalliferous
551 sediment core from the Mid-Atlantic Ridge. *J. Geophys. Res.*, 98:9671-9681.
- 552 Muiños, S.B., Frank, M., Maden, C., Hein, J.R., van de Flierdt, T., Lebreiro, S.M., Gaspar, L., Monteiro, J.H., Halliday,
553 A.N., 2008. New constraints on the Pb and Nd isotopic evolution of NE Atlantic water masses. *Geochemistry,*
554 *Geophysics, Geosystems* 9, 18.
- 555 Nicholson, K. 1992. Contrasting mineralogical-geochemical signatures of manganese oxides: guides to metallogenesis.
556 *Econ. Geol.* 87, 1253–1264.
- 557 Okay, A.I., Simmons, M., Özcan, E., Starkie, S., Bidgood, M. & Kylander-Clark, A.R.C., 2020, Eocene-Oligocene
558 succession at Kızılköy (Midye) on the Black Sea coast in Thrace. *Turkish Journal of Earth Sciences*, 29, 139-153.
- 559 Oygür, V., 1990. Çayırılı (Ankara-Haymana) manganez yatağının jeolojisi ve kökeni üzerine görüşler. *MTA Dergisi* 110,
560 29–44 (in Turkish).

- 561 Riding, R., Fralick, P., Liang, L., 2014. Identification of an Archean marine oxygen oasis. *Precambrian Res.* 251, 232–237.
- 562 Roy A, Chakrabarti G, Shome D. 2018. Geochemistry of the Neoproterozoic Narji limestone, Cuddapah Basin, Andhra
563 Pradesh, India: implication on palaeoenvironment. *Arab J Geosci* 11, 784–796
- 564 Sasmaz, A., Turkyılmaz, B., Ozturk, N., Yavuz, F., Kumral, M. 2014. Geology and geochemistry of Middle Eocene Maden
565 complex ferromanganese deposits from the Elazığ-Malatya region, eastern Turkey. *Ore Geol. Rev.* 56, 352–372.
- 566 Sasmaz A, Kryuchenko N, Zhovinsky E, Suyarko V, Konakci N, Akgul B. 2018. Major, trace and rare earth element (REE)
567 geochemistry of different colored fluorites in the Bobrynets region, Ukraine. *Ore Geology Reviews* 102, 338-350.
- 568 Schmidt, K., Bau, M., Hein, J.R., Koschinsky, A. 2014. Fractionation of the geochemical twins Zr/Hf and Nb/Ta during
569 scavenging from sea water by hydrogenetic ferromanganese crusts. *Geochim. Cosmochim. Acta*, 140, 468-487.
- 570 Schwinn, G., Markl, G. 2005. REE systematics in hydrothermal fluorite. *Chem. Geol.* 216, 225–248.
- 571 Selin Y.I., 1984. Stratigraphy and mollusks of the Oligocene of Bolshoi Tokmak manganese ore region. Moscow: Nedra,
572 240 p.
- 573 Shah, M.T., Moon, C.J. 2007. Manganese and ferromanganese ores from different tectonic settings in the NW Himalayas,
574 Pakistan. *J. Asian Earth Sci.* 29, 455–465.
- 575 Sinanoglu, D., Sasmaz, A. 2019. Geochemical evidence on the depositional environment of Nummulites accumulations
576 around Elazığ, Sivas, and Eskişehir (Turkey) in the middle Eocene sub-epoch. *Arabian J. Geoscience*. 12:759.
- 577 Slack, J., Grenne, T., Bekker, A., Rouxel, O., Lindberg, P., 2007. Suboxic deep seawater in the late Paleoproterozoic:
578 evidence from hematitic chert and iron formation related to seafloor hydrothermal sulfide deposits, central Arizona,
579 USA. *Earth Planet. Sci. Lett.* 255, 243–256.
- 580 Sokal, R.R. Rohlf, F.J. 1995. *Biometry: The Principles and Practice of Statistics in Biological Research*, third ed.. W.H.
581 Freeman and Co, New York, p 887.
- 582 Strishkov, V., Levine, R.M. 1987. *The Manganese Industry of the U.S.S.R.* Washington, DC: U. S. Bureau of Mines/U. S.
583 Government Printing Office.
- 584 Sun, S.-S., 1980. Lead isotopic study of young volcanic rocks from midocean ridges, ocean islands and island arcs. *Philos.*
585 *Trans. R. Soc. London. A*, 297:409-445.
- 586 Strakhov, N.M., Shterenberg, L.E., Kalinenko, V.V. and Tikhomirova, Z.S. 1968. Geochemistry of manganese ore
587 sedimentation, *Tr.Geol. Inst. AN SSSR*, 185, 495 p. (in Russian).
- 588 Takahashi, Y., Hirata, T., Shimizu, H., Ozaki, T., Fortin, D., 2007. A rare earth element signature of bacteria in natural
589 waters? *Chem. Geol.* 244, 569–583.
- 590 Taylor S. R. and McLennan S. M. 1985. *The Continental Crust: Its Composition and Evolution*. Blackwell, Oxford.
- 591 Tobia, F.H. 2018. Stable isotope and rare earth element geochemistry of the Baluti carbonates (Upper Triassic), Northern
592 Iraq. *Geosci J* 22 (6), 975–987
- 593 Tostevin, R., Shields, G.A., Tarbuck, G.M., He, T., Clarkson, M.O., Wood, R.A., 2016. Effective use of the cerium
594 anomalies as a redox proxy in carbonate-dominated marine settings. *Chem. Geol* 438, 146–162.
- 595 Toth, J.R., 1980. Deposition of submarine crusts rich in manganese and iron. *Geol. Soc. Am. Bull.* 91, 44–54.
- 596 Turekian, K.K., Wedepohl, K.H. 1961. Distribution of elements in some major units of earth's crust. *Geol Soc Am Bull* 72,
597 175–192.
- 598 Varentsov, I.M. 1964. *Sedimentary Manganese Ores*. Elsevier. Amsterdam
- 599 Varentsov, I. M., and Rakhmanov, V. P., 1977. Deposits of Manganese. In Smirnov V.I. (ed.), *Ore Deposits of the USSR*,
600 Vol. 1, 114-178 Pitman, London.

601 Varentsov, I. M., and Rakhmanov, V. P., 1980. Manganese deposits of the USSR (A review), *in* Varentsov, I. M., and
602 Grasselly, GY., eds., *Geology* 319-391

603 Varentsov, I.M. 2002. Genesis of the eastern Paratethys manganese ore giants. Impact of events at the Eocene/Oligocene
604 boundary. *Ore Geology Reviews* 20: 65-82

605 Vereshchagin, O. S., Perova, E. N., Brusnitsyn, A. I., Ershova, V. B., Khudoley, A. K., Shilovskikh, V. V., Molchanova,
606 E.V. 2019. Ferro-manganese nodules from the Kara Sea: mineralogy, geochemistry and genesis. *Ore Geol.*
607 *Rev.* 106, 192–204.

608 von Blanckenburg, F., O’Nions, R.K., Hein, J.R. 1996. Distribution and sources of pre-anthropogenic lead isotopes in deep
609 ocean water from Fe-Mn crusts, *Geochim. Cosmochim. Acta*, 60, 4936– 4957,

610 von Blackenburg, F., Nägler, T.F., 2001. Weathering versus circulation-controlled changes in radiogenic isotope tracer
611 composition of the Labrador Sea and northAtlantic deep water. *Paleoceanography* 16, 424–434

612 Wang, C.M., Deng, J., Carranza, E.J.M., Lai, X.R., 2014. Nature, diversity and temporal–spatial distributions of sediment-
613 hosted Pb–Zn deposits in China. *Ore Geol. Rev.* 56, 327–351

614 Zeng, Z., Ouyang, H., Yin, X., Chen, S., Wang, X., Wua, L., 2012. Formation of Fe–Si–Mn oxyhydroxides at the
615 Pacmanuss hydrothermal field, Eastern Manus Basin: mineralogical and geochemical evidence. *J. Asian Earth Sci.*
616 60, 130–146.

617
618
619
620
621
622
623
624
625
626
627
628
629
630
631
632
633
634
635
636
637
638
639
640
641
642

Figure File.



Fig. 1. Map showing location of Chiaturn and other Oligocene manganese deposits and simplified regional paleogeography setting of the Early Oligocene of the Eastern Paratethys (Changed from Okay et al., 2020).

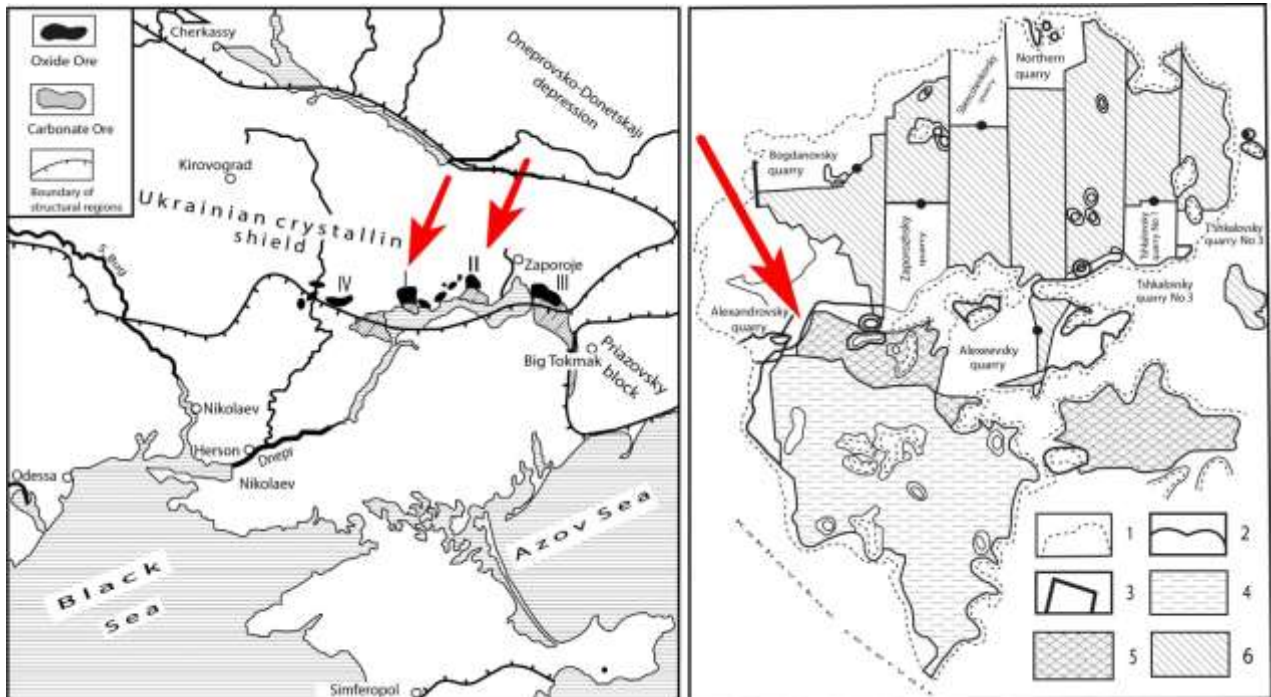


Fig. 2. Structural position of Mn deposits in the Nikopol ore basin (Selin, 1984); 1—boundary of ore bodies; 2—isoline of thickness 0.75m. ore body; 3—boundaries of mining areas; 4—carbonate, 5—oxide-carbonate, 6—oxide.



Fig. 4. Oxide-hydroxide ore zone in Nikopol manganese deposit



Fig. 5. Oxide-hydroxide ores (black) in mixed oxide-carbonate ore zone

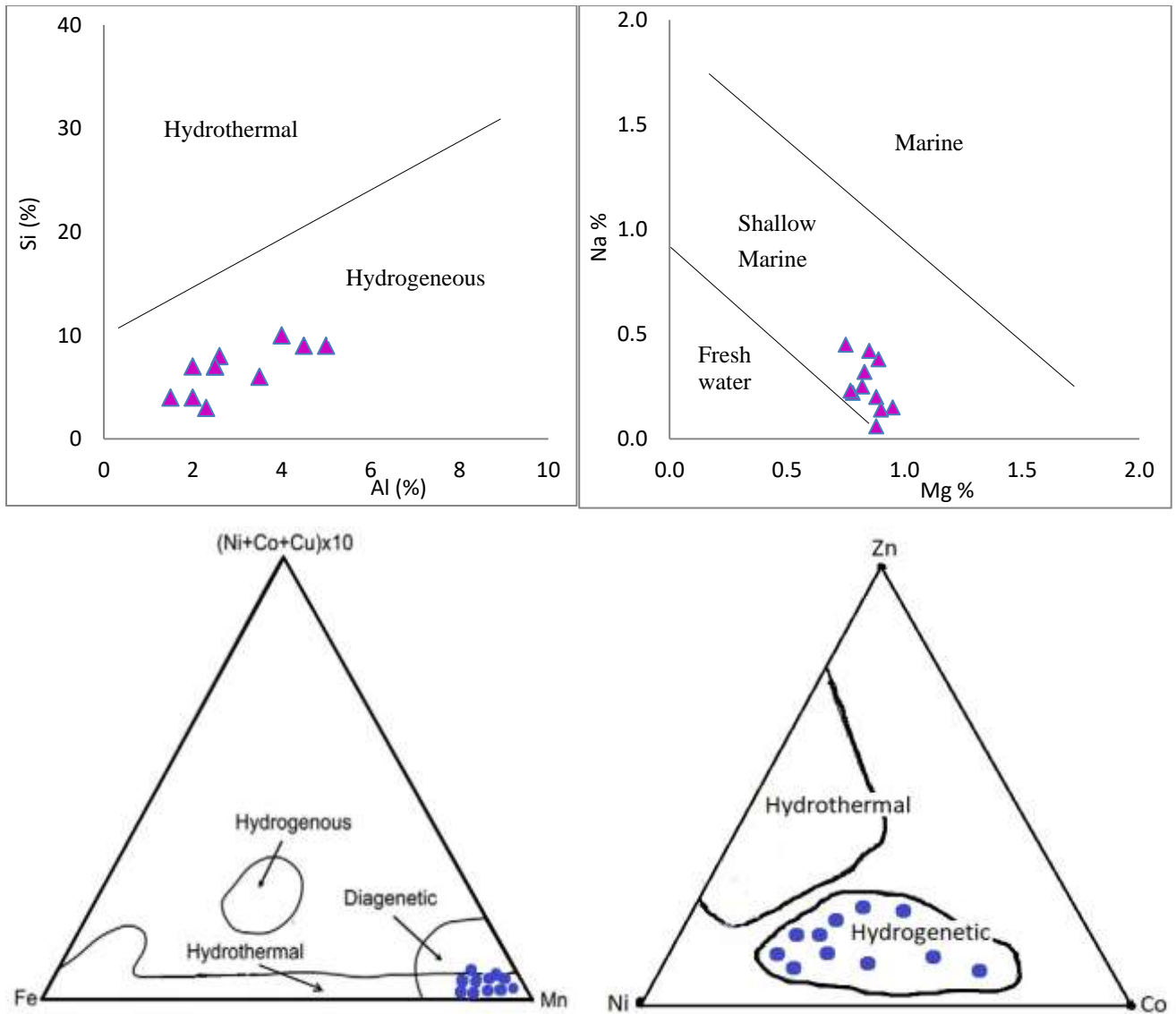


Fig. 5. Discrimination diagrams for the Nikopol manganese oxides Al-Si (Choi and Hariya, 1992), Mg-Na (Nicholson, 1992), Mn-Fe-(Ni + Co + Cu)x10 (Bonatti et al., 1972; Crerar et al., 1982) and Ni-Zn-Co (Choi and Hariya, 1992).

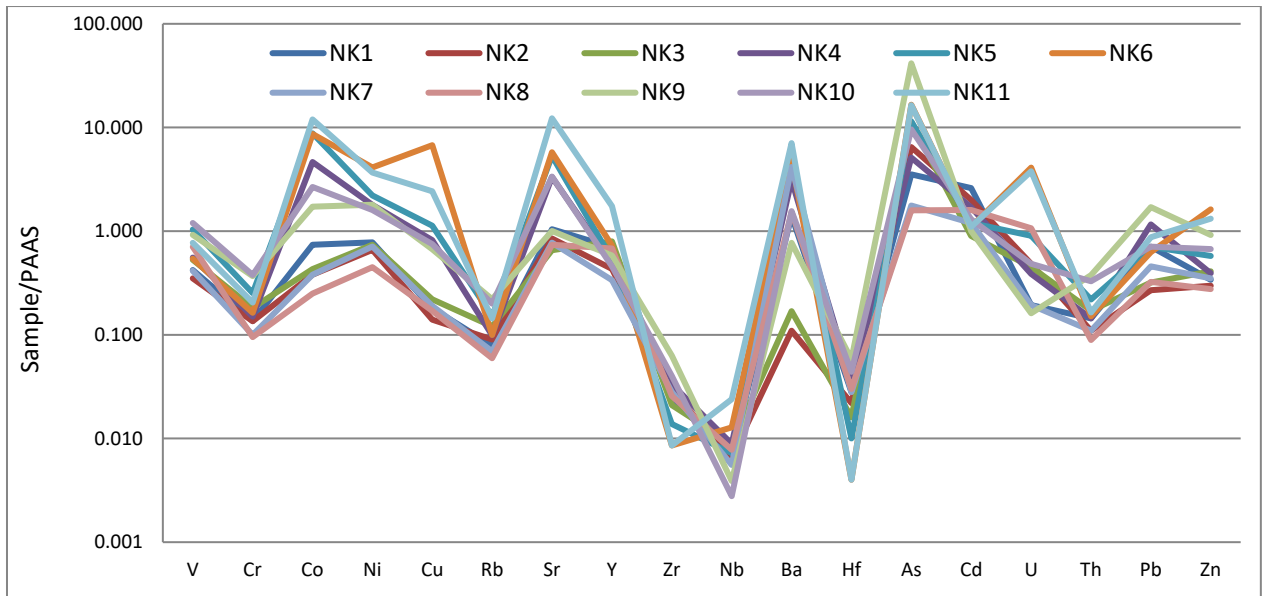


Fig. 6. Post Archean Australian Shale (PAAS)-normalized trace element distribution of Nikopol manganese oxides; PAAS data from Taylor and McLennan (1985).

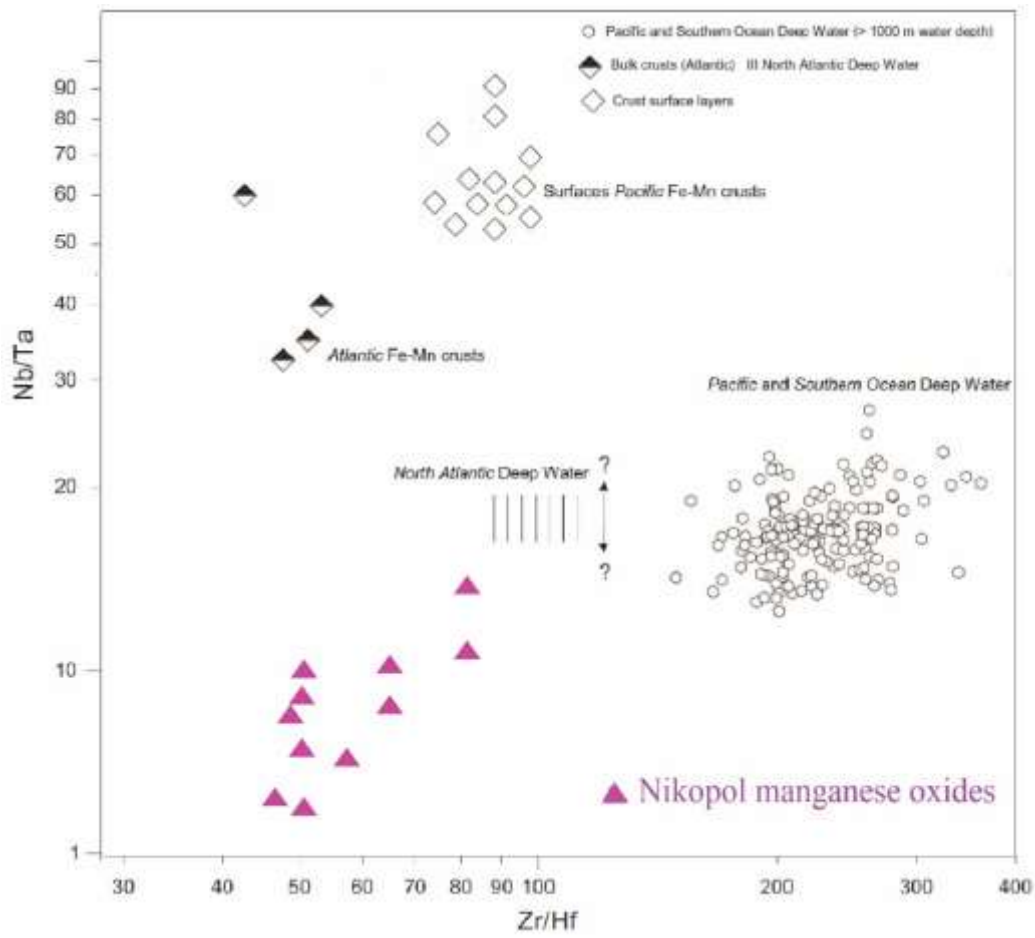


Fig. 8. Nb/Ta and Zr/Hf ratios in Nikopol manganese oxides compared to other oxide deposits (modified from Schmidt et al., 2014; North Atlantic Deep Water, Godfrey et al., 1996, 2009; Arctic and Pacific Deep Water, Firdaus et al., 2011).

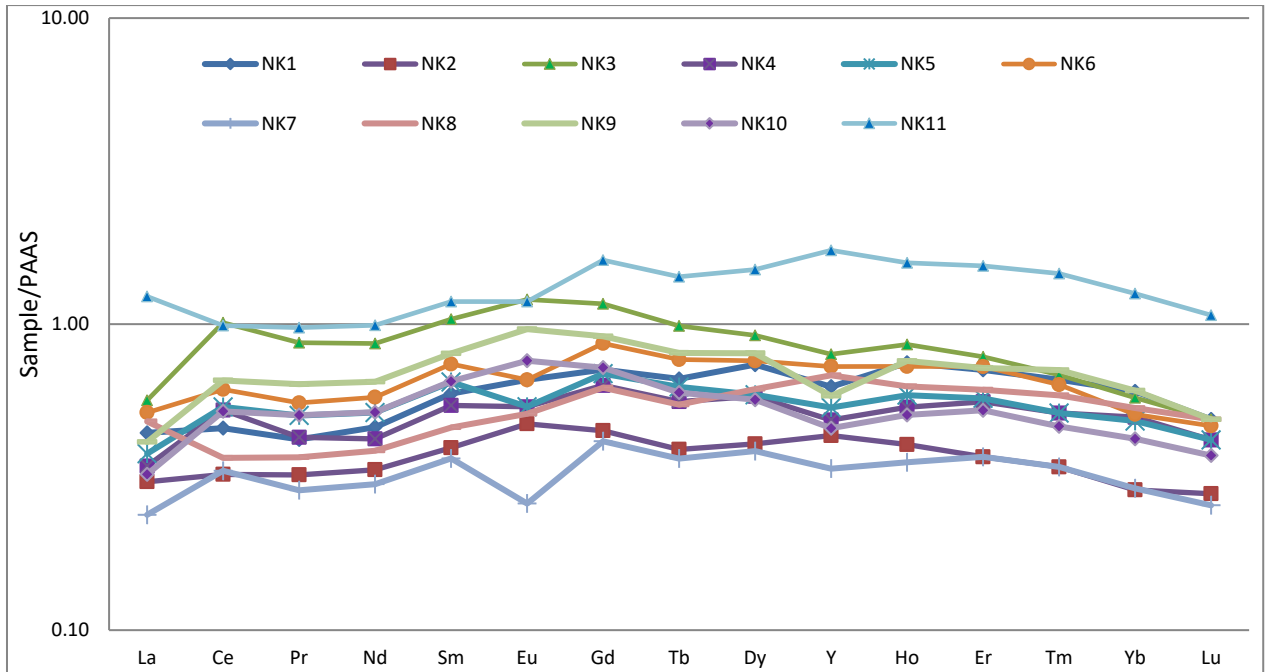


Fig. 8. PAAS normalized REE + Y patterns of the Nikopol manganese samples; PAAS composition from Taylor and McLennan (1985).

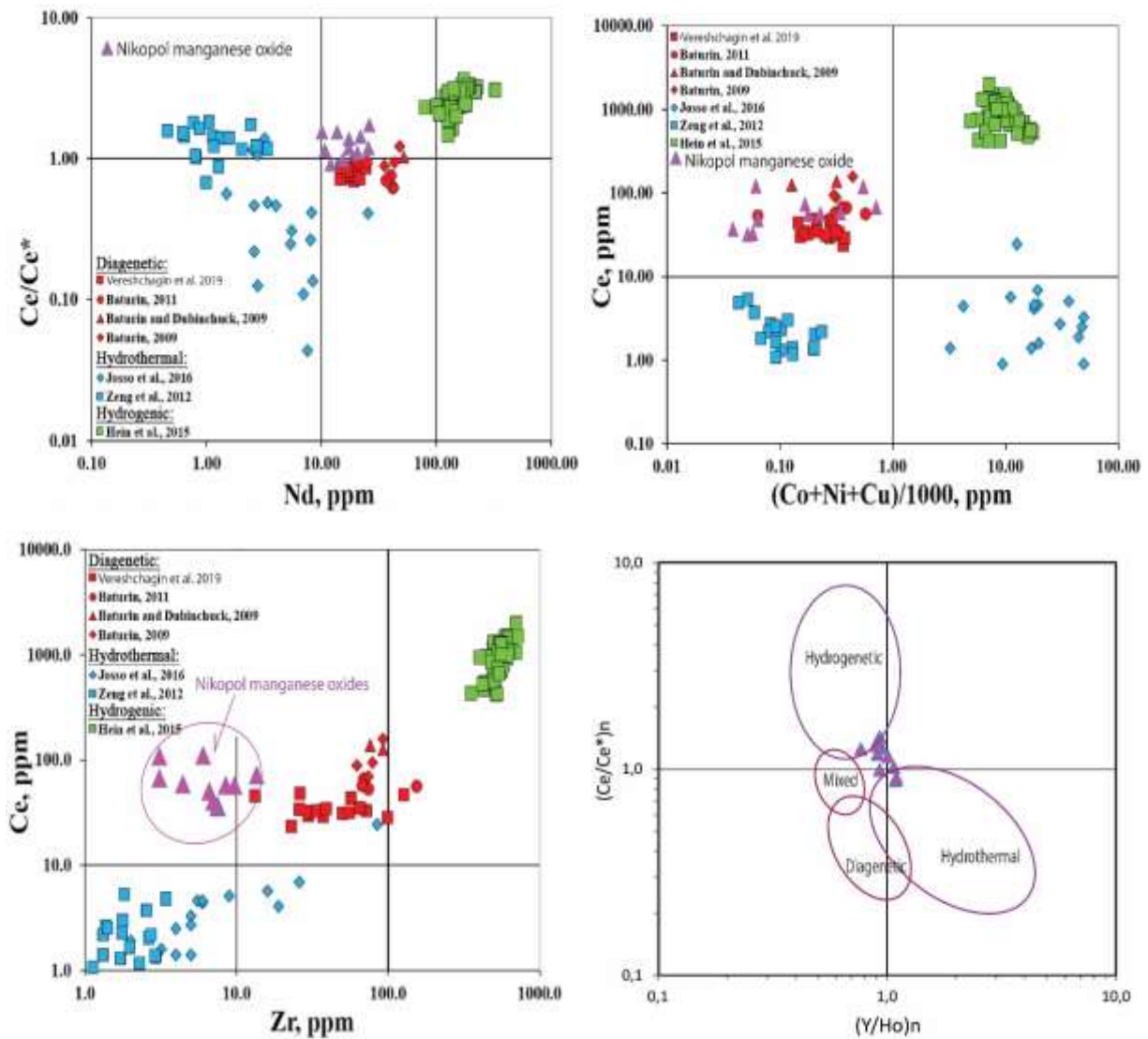


Fig. 9. Different genetic types of Mn deposits in a) Ce/Ce^* ratio vs Nd concentration (after Bau et al., 2014; Baturin, 2009, 2011; Baturin and Dubinchuck, 2009); b) Ce vs $(Co+Ni+Cu)/1000$ ratios, from Zeng et al. (2012), Hein et al. (2015), Joso et al. (2017) and Vereshchagin et al. (2019); c) Ce vs Zr ratios (data in Fig 9a,b,c; from Vereshchagin et al., 2019); and d) Ce/Ce^* vs $(Y/Ho)_n$ diagram (from Bau et al. (2014)). The ferromanganese concretions of the Kara Sea (Baturin, 2011), ferromanganese nodules in the Gulf of Finland, Baltic Sea (Baturin, 2009), ferromanganese nodules from Riga Bay from Baturin and Dubinchuck (2009) and Ferro-manganese nodules from the Kara Sea (Vereshchagin et al., 2019).

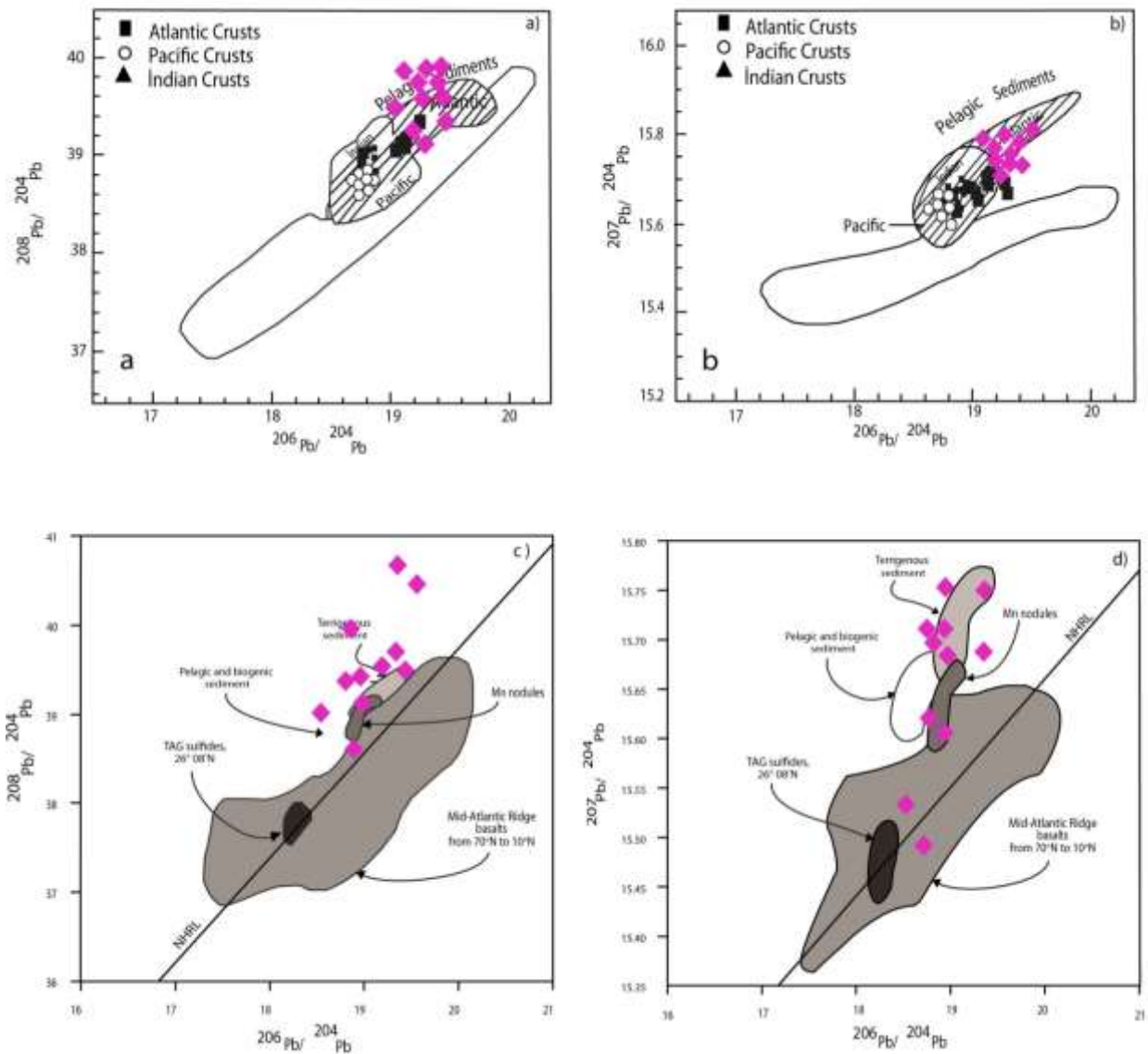


Fig. 10. a) and b) Comparison of Pb isotope ratios for MORB and pelagic sediments with those from Fe-Mn crusts (taken from von Blanckenburg et al., 1996); c and d) diagrams for the Mid-Atlantic Ridge basalts (Sun, 1980; Hamelin et al., 1984; Ito et al., 1987; Dosso et al., 1991, 1993), Atlantic sediments (Ben Othman et al., 1989), and Mn nodules (Ben Othman et al., 1989; Mills et al., 1993; Godfrey et al., 1994). NHRL = the Northern Hemisphere Reference Line according to Hart (1984) (taken from Andrieu et al., 1998).

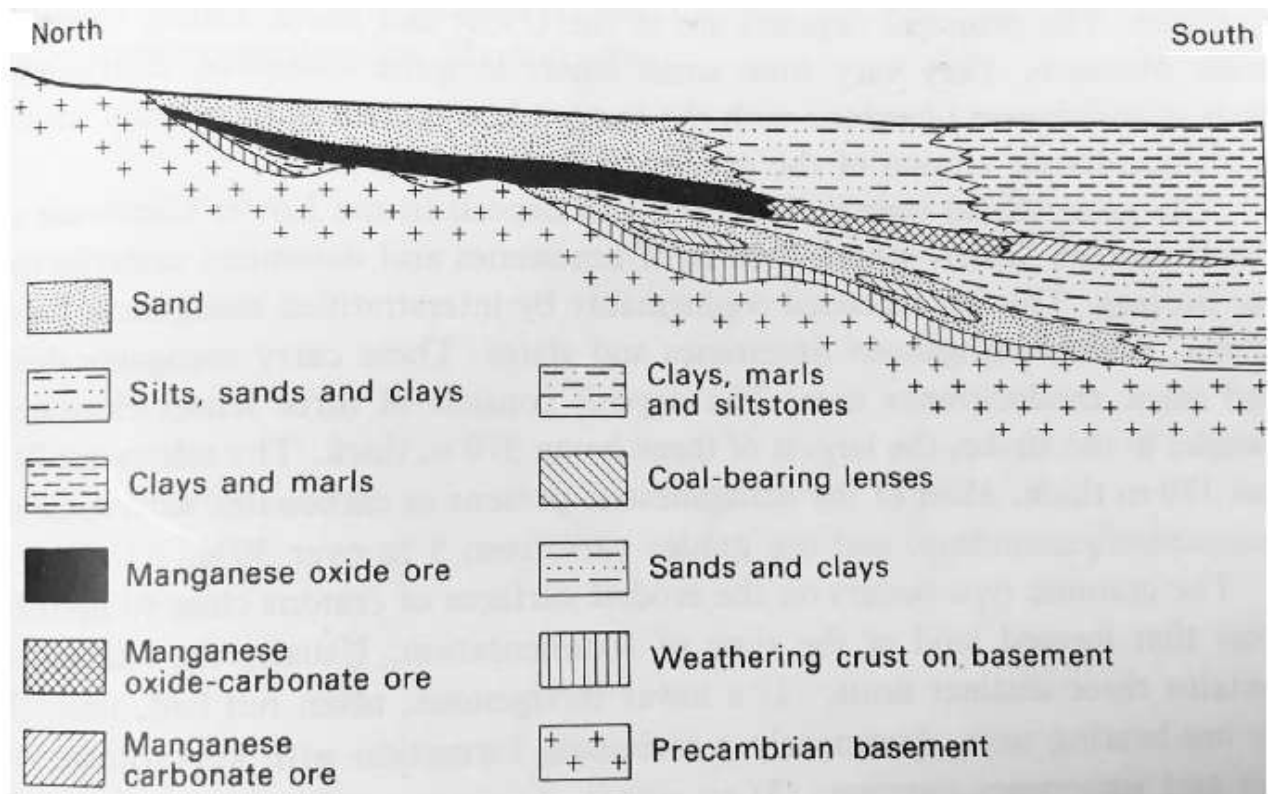


Fig. 11. Cross section through the Nikopol manganese deposit showing the zonation of the manganese ores and transgressive nature of the sedimentary sequence with its overlap on to the Precambrian basement of the Ukrainian Platform (after Varentsov, 1964)

Table 1. Major oxide contents (%) of Nikopol manganese oxide ores.

Sample	SiO ₂	Al ₂ O ₃	Fe ₂ O ₃	MgO	CaO	Na ₂ O	K ₂ O	TiO ₂	P ₂ O ₅	MnO	Cr ₂ O ₃	LOI	Sum	Mn	Fe	Mn/Fe	Al	Si
NK1	16,85	3,89	2,91	1,23	9,62	0,46	0,7	0,15	0,33	42,6	0,004	20,4	99,1	33	1,99	16,6	2,07	7,87
NK2	7,46	3,72	3,94	1,27	4,25	0,31	0,61	0,14	0,33	44,4	0,005	32,8	99,2	34,4	2,7	12,8	1,98	3,49
NK3	17,85	3,6	4,48	1,45	8,03	0,25	0,77	0,18	0,66	32,4	0,006	29,3	99,1	25,1	3,07	8,2	1,91	8,34
NK4	15,27	3,25	4,62	1,33	8,34	0,36	0,93	0,17	0,26	36,1	0,005	28,3	98,9	28	3,16	8,8	1,73	7,14
NK5	21,6	5,05	3,63	1,36	6,24	0,67	0,49	0,26	0,38	37,6	0,008	22	99,4	29,2	2,49	11,7	2,69	10,09
NK6	14,08	4,72	3,64	1,35	3,03	0,45	0,88	0,12	1,07	54,5	0,005	14,5	98,3	42,2	2,49	16,9	2,51	6,58
NK7	10,54	2,04	4,53	1,26	10,5	0,08	0,45	0,1	0,26	38,1	0,004	32,1	99,9	29,5	3,1	9,5	1,09	4,93
NK8	9,61	2,73	3,33	1,01	10,3	0,32	0,38	0,09	0,37	38,4	0,004	32,9	99,5	29,8	2,28	13,1	1,45	4,49
NK9	20,7	6,41	4,49	1,35	7,1	0,2	1,55	0,38	0,24	36,1	0,01	21,2	99,7	28	3,08	9,1	3,41	9,67
NK10	20,97	6,88	3,76	1,28	4,21	0,55	1,88	0,4	0,19	40,7	0,01	18,5	99,4	31,6	2,58	12,3	3,66	9,8
NK11	16,47	3,59	5,73	1,22	6,16	0,57	1,12	0,17	2,29	46,9	0,006	14,8	99,1	36,3	3,92	9,3	1,91	7,7
Avrg	15,58	4,17	4,10	1,27	7,07	0,38	0,89	0,20	0,58	40,7	0,006	24,3	99,2	31,5	2,805	11,67	2,22	7,28

1 Table 2: Trace element concentrations (ppm) of Nikopol manganese deposit (TTE: Total trace element).

	V	Cr	Co	Ni	Cu	Rb	Sr	Y	Zr	Nb	Ba	Hf	As	Cd	U	Th	Pb	Zn	TTE	Mn/Fe	Co/Ni	Co/Zn	Zr/Hf	Co+Ni+Cu	(Ni+Co+Cu)*10	Nb/Ta	
NK1	59	13,6	14,8	43,6	8,9	12,6	209	18,9	5,0	0,13	895	0,14	6,0	0,26	0,6	2,1	14,2	28,8	1333	6,2	0,34	0,51	35	543	673	6,5	
NK2	49	13,5	7,6	39,4	7,10	14,4	170	11,7	6,0	0,12	70	0,11	11,0	0,20	1,5	1,6	5,4	25,3	433	6,5	0,19	0,30	54	305	541	3,0	
NK3	74	18,2	8,6	44,1	10,9	19,3	131	21,5	4,4	0,16	108	0,08	19,1	0,09	1,4	2,5	6,4	34,8	504	9,5	0,20	0,25	75	668	636	5,3	
NK4	78	15,0	93,0	107	41,2	15,8	664	13,1	7,0	0,16	1974	0,18	8,7	0,17	1,2	2,1	23,2	33,4	3078	35	0,87	2,78	62	631	2413	8,0	
NK5	145	25,3	176	132	56,6	24,1	1065	14,4	2,9	0,13	3081	0,05	19,5	0,12	2,8	3,2	14,1	49	4811	39	1,32	3,58	70	357	3646	6,5	
NK6	76	16,3	173	246	337	15,9	1152	19,6	1,8	0,23	3085	0,02	28,2	0,11	12,7	2,2	12,6	138	5318	15	0,70	1,25	70	1472	7566	7,7	
NK7	58	10,0	7,5	42,5	9,57	11,1	155	9,10	5,9	0,10	2644	0,14	3,0	0,12	0,6	1,6	9,2	29,8	2997	38	0,18	0,25	58	446	596	3,3	
NK8	99	9,5	4,9	26,8	8,26	9,5	148	18,4	5,4	0,14	973	0,15	2,7	0,16	3,3	1,3	6,5	23,5	1340	43	0,18	0,21	45	1006	400	7,0	
NK9	129	36,8	34,3	108	33,6	35,3	201	15,7	13,2	0,07	491	0,29	70,7	0,10	0,5	5,5	34,1	78	1287	47	0,32	0,44	83	745	1758	2,3	
NK10	168	37,7	53,4	96,6	37,6	32,0	673	12,3	8,4	0,05	991	0,22	16,3	0,13	1,5	4,8	14,2	57	2205	26	0,55	0,94	33	320	1876	2,5	
NK11	108	20,5	239	221	121	23,0	2453	47,1	1,8	0,43	4491	0,02	27,9	0,11	11,7	2,4	17,5	112	7897	10	1,08	2,13	43	296	5804	14,3	
Average	94,8	19,7	73,7	101	61,1	19,4	638	18,4	5,62	0,16	1709	0,13	19,4	0,14	3,44	2,66	14,3	55,4	2836	25	0,54	1,15	57	617	2355	6,0	
PAAS	140	100	20	60	50	160	200	27	210	18	636	5	1,7	0,1	3,1	14,6	20	85									

2
3
4
5
6
7

Table 3. Major and trace element contents of various types of manganese deposits. Analyses taken from (1) = (Shah and Moon, 2007), (2, 3, 4, 5) = (Choi and Hariya, 1992), (6) = (Gultekin and Balci, 2008), (7) = (Oygür, 1990), (8) = (Koç et al., 2000) and (9)= (Sasmaz et al., 2014).

Countries	Pakistan (1)	Japan (2)	Japan (3)	Japan (4)	Japan (5)	Turkey (6)	Turkey (7)	Turkey (8)	Turkey (9)	This study ⁹
Regions	Hazara	Wakasa	Koryu	Hinode	Tokora	Binkılıç	Çayırılı	Kasımağa	Maden Complex	Nikopol ¹⁰
Orig ins	Hydrothermal/ hydrogenous	Hydrothermal	Hydrothermal	Sedimentary	Sedimentary	Sedimentary	Volcano- sedimentary	Volcano- sedimentary	Sedimentary exhalative	Sedimentary ¹¹
SiO ₂ (%)	9,41	58,16	40,56	12,7	32	9,69	63	13,4	24,6	15,9 ¹²
TiO ₂ (%)	0,84	0,04	0,05	0,04	0,91	0,30	0,03	0,10	0,14	0,20 ¹³
Al ₂ O ₃ (%)	12,5	0,55	0,63	1,27	8,82	1,39	0,65	2,95	3,62	4,17 ¹⁴
Fe ₂ O ₃ (%)	20,3	0,92	0,55	0,59	38,3	3,69	0,68	14	33,7	4,10 ¹⁴
MnO (%)	33,78	32,5	42,06	67,2	5,22	53,2	29,2	40	11,6	40,7 ¹⁵
MgO (%)	0,59	0,19	0,02	0,08	4,04	1,12	0,2	12,7	1,23	1,26 ¹⁶
CaO (%)	6,43	4,15	1,65	1,67	8,82	16,6	0,24	6,82	9,78	7,07 ¹⁷
Na ₂ O (%)	0,07	0,04	0,11	0,07	0,82	0,43	0,05	0,06	0,1	0,38 ¹⁷
K ₂ O (%)	0,88	0,1	0,27	0,46	0,26	0,34	0,11	0,19	0,04	0,89 ¹⁸
P ₂ O ₅ (%)	3,73	0,1	0,02	0,12	0,62	0,97	0,04	0,08	1,35	0,58 ¹⁹
Ba (ppm)	6304	13,79	22126	8,1	99	2125	1229	2719	625	1938 ²⁰
V (ppm)	573	258	211	468	1637	39,8	144	106	874	95 ²⁰
Cr	247	10	7	16	186	13,6	13,7	10	18	20 ²¹
Co	404	2	118	222	433	73,6	25,2	49,5	68,4	74 ²²
Ni	305	28	351	341	432	125	69,4	23	662	101 ²³
Cu	375	50	1174	691	500	95,6	154,9	126,8	553	61 ²³
Zn	580	26	129	147	374	60	66,7	63,5	288	55,4 ²⁴
Pb	2357	112	14	18	267	41	6,5	53,5	115	14,3 ²⁵
Th	31	2	2	98	4	-	0,4	433	2,45	2,66 ²⁵
Rb	24	2	3	4	5	18	2,9	5	1,62	19 ²⁶
Sr	-	85	483	260	102	2664	243	255	588	638 ²⁷
Y	-	5	-	-	80	14,8	33	22	136	18,4 ²⁸
Nb	-	3	8	4	4	-	0,7	11,1	3,94	0,16 ²⁸
Zr	-	12	62	48	104	49,4	4	26,9	88	5,62 ²⁹

30

31 Table 4. Rare earth element contents (ppm) and Pb isotope ratios of the Nikopol manganese oxide deposits.

32

	Y	La	Ce	Pr	Nd	Sm	Eu	Gd	Tb	Dy	Ho	Er	Tm	Yb	Lu	ΣREE	(Ce/Ce*) _n	(Eu/Eu*) _n	(Y/Y*) _n	(Pr/Pr) _{nn}	(La/Yb) _n	(Y/Ho) _n	²⁰⁸ Pb/ ²⁰⁴ Pb	²⁰⁷ Pb/ ²⁰⁴ Pb	²⁰⁶ Pb/ ²⁰⁴ Pb
NK1	18,9	16,6	38,4	3,87	15,6	3,29	0,71	3,31	0,51	3,45	0,74	2,02	0,27	1,70	0,21	91	0,99	1,03	0,83	0,95	0,73	0,84	39,24	15,72	18,92
NK2	11,7	14,7	25,7	2,84	11,3	2,19	0,51	2,09	0,30	1,90	0,40	1,05	0,14	0,81	0,12	64	1,02	1,12	1,04	0,94	1,06	1,07	39,56	15,68	19,04
NK3	21,5	38,9	80,5	7,68	29,3	5,76	1,30	5,43	0,76	4,30	0,85	2,23	0,28	1,62	0,21	179	1,43	1,09	0,90	1,01	0,98	0,93	38,94	15,65	19,03
NK4	13,1	17,5	41,7	3,77	14,3	3,01	0,58	2,94	0,43	2,72	0,53	1,59	0,21	1,40	0,18	91	1,37	0,93	0,88	0,92	0,69	0,91	39,45	15,64	18,88
NK5	14,4	18,9	42,7	4,44	17,4	3,59	0,58	3,21	0,48	2,75	0,58	1,63	0,21	1,36	0,18	98	1,18	0,81	0,90	0,95	0,78	0,91	39,58	15,66	18,98
NK6	19,6	22,2	48,7	4,88	19,6	4,11	0,71	4,03	0,59	3,55	0,72	2,07	0,26	1,43	0,20	113	1,15	0,83	0,96	0,93	1,01	1,00	38,64	15,67	18,82
NK7	9,1	12,4	26,4	2,53	10,2	2,02	0,28	1,93	0,28	1,80	0,35	1,05	0,14	0,82	0,11	60	1,27	0,68	0,92	0,94	0,82	0,95	38,82	15,73	19,22
NK8	18,4	18,2	29,1	3,24	13,1	2,55	0,55	2,89	0,42	2,87	0,62	1,74	0,24	1,50	0,21	77	0,88	0,96	1,10	0,97	0,90	1,09	39,25	15,66	19,10
NK9	15,7	23,4	52,1	5,62	21,9	4,45	1,04	4,25	0,62	3,76	0,75	2,05	0,29	1,71	0,21	122	1,25	1,18	0,75	0,98	0,68	0,77	39,66	15,70	19,08
NK10	12,3	18,5	41,3	4,45	17,5	3,61	0,82	3,36	0,46	2,65	0,50	1,49	0,19	1,19	0,16	96	1,30	1,12	0,85	0,96	0,77	0,90	39,60	15,69	18,76
NK11	47,1	41,5	78,7	8,60	33,6	6,58	1,28	7,54	1,10	7,06	1,57	4,42	0,60	3,55	0,46	197	0,91	0,86	1,12	0,98	0,98	1,10	39,12	15,71	18,68
Average	18,2	22,3	45,8	4,72	18,5	3,74	0,76	3,73	0,54	3,35	0,69	1,94	0,26	1,55	0,20	108	1,16	0,96	0,93	0,96	0,86	0,95	39,4	15,7	19,0
PAAS	38,2	79,6	8,83	33,9	5,55	1,08	4,66	0,77	4,68	27,00	0,99	2,85	0,41	2,82	0,43	212									

33

34

35

36